Yoder, Jr., P.R. “Optical Mounts: Lenses, Windows, Small Mirrors, and Prisms”
Optomechanical Engineering Handbook
Ed. Anees Ahmad
Boca Raton: CRC Press LLC, 1999

Optical Mounts: Lenses, Windows, Small Mirrors, and Prisms

Paul R. Yoder, Jr.

6.1 Introduction and Summary

A variety of common techniques for mounting optical components such as individual and multiple lenses, windows, domes, filters, small mirrors, and prisms are discussed here. Numerous examples from the literature illustrate these techniques. Analytical relationships are given for estimating selected important attributes of the designs such as contact stress due to forces imposed during assembly or due to temperature changes or acceleration. Principles of optomechanical design and material selection intended to minimize the adverse effects of these imposed forces while retaining component function, location, and alignment are explained.

6.2 Mounting Lenses

Low Precision Mounts

In this section, configurations for relatively low cost, low precision mounts for lenses are considered. In each case, the parts are premachined to specified dimensions and assembled without adjustment. Although the examples show single lens elements, some of these concepts are applicable to multiple element designs. For simplicity, it is assumed in most cases that the lenses are glass and the mount is a simple, cylindrical metal cell.

Spring Suspension

In applications involving large temperature changes with loose centration, tilt, and/or axial positioning tolerances, lenses might be supported by springs.[1,2] One such mounting, typically used to support condenser lenses or filters made of heat-absorbing glass in projector illuminators, is illustrated in Figure 6.1. Three flat springs spaced at 120° intervals around the lens rim are shaped to interface with that rim. Symmetry of the cantilevered springs tends to keep the lens centered. Free circulation of air around the lens is allowed. This type of mount also offers some protection against shock and vibration.

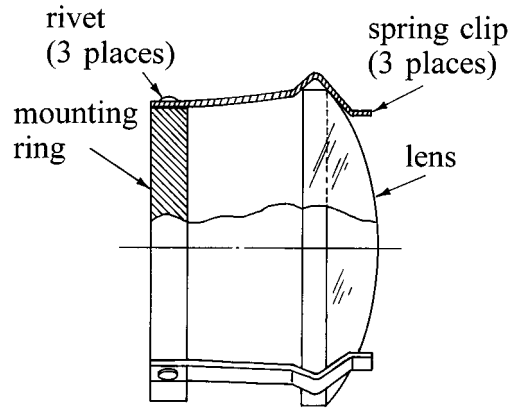

FIGURE 6.1 Typical configuration of a spring-mounted lens element. (From Yoder, P.R., Jr. 1993. *Opto-Mechanical Systems Design*, 2nd ed. Marcel Dekker, New York.)

Interference-Fit Ring

A lens can be held against a shoulder or spacer in a cell by an axial force exerted against the lens near its rim by a continuous ring as shown in Figure 6.2. The outside diameter (OD) of the ring is made slightly oversize with respect to the inside diameter (ID) of the cell. After installing the lens, the ring can be pressed into place or (preferably) the ring shrunk by cooling and inserted into a cell expanded by heating. The cell and ring materials should have similar thermal expansion coefficients to prevent loosening at extreme temperatures.

It is difficult to determine exactly when the ring touches the lens surface during assembly so achievement of a particular axial force on the lens is difficult.[2] Assembly by this technique is essentially permanent since it is virtually impossible to remove the ring without damaging either it or the lens.

Snap Ring

A discontinuous ring that drops into a groove machined into the inside surface of a cell is commonly termed a "snap" ring.[1-3] This ring, which acts as a spring, usually has a circular cross section as shown in Figure 6.3. Rectangular cross-section rings are less frequently used. The opening or slot

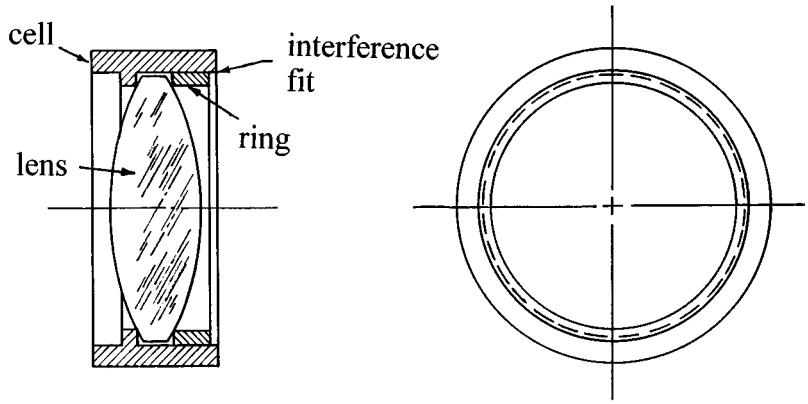

FIGURE 6.2 Typical configuration of a lens held in place by a pressed-in-place continuous ring. (Adapted from Yoder, P.R., Jr. 1993. *Opto-Mechanical Systems Design*, 2nd ed. Marcel Dekker, New York.)

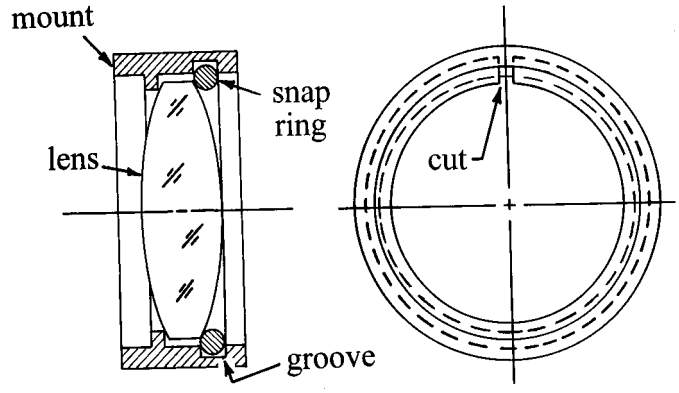

FIGURE 6.3 Typical configuration of a lens held in place by a discontinuous snap ring with circular cross section. (From Yoder, P.R., Jr. 1993. *Opto-Mechanical Systems Design*, 2nd ed. Marcel Dekker, New York.)

in the ring allows it to be compressed slightly while sliding into alignment with the groove. The groove cross section is usually rectangular.

Ensuring contact between the lens surface and the ring using this technique is difficult since thickness, diameter, and surface radius of the lens as well as ring dimensions, groove location, dimensions, and temperature changes all affect the degree of mechanical interference, if any, existing between the lens and ring. For this reason, this technique is used only where the location and orientation of the lens is not critical. Provision of a specific axial restraining force to the lens with this type mount is virtually impossible.

If the cell is designed without a groove, a snap ring can be inserted against the lens and constraint offered by friction between the ring and cell wall.[1] A rectangular ring is preferred in this case. Disassembly is possible. This design is sensitive to shock and vibration.

Burnished Cell

If the cell is made of malleable material such as brass or certain aluminum alloys, it can be designed to be mechanically deformed around the rim of a lens at assembly so as to secure that lens against an internal cell shoulder or spacer.[1,2,4] Figure 6.4 illustrates a typical example. At left is shown the cell prior to assembly. The chucking thread allows the cell to be installed onto a lathe spindle. In some designs, the cell lip is tapered to facilitate intimate contact with the lens bevel.

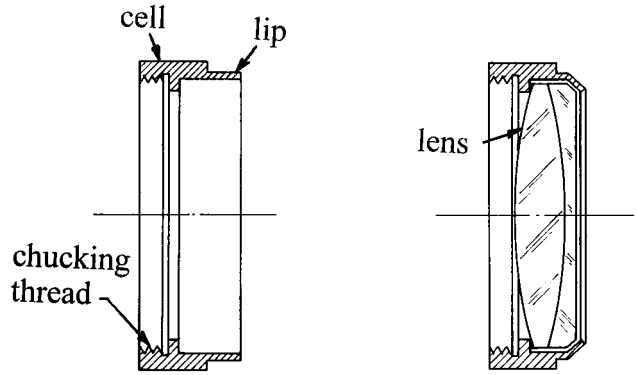

FIGURE 6.4 Typical configuration of a lens held in place by burnishing the cell rim. (From Yoder, P.R., Jr. 1993. *Opto-Mechanical Systems Design*, 2nd ed. Marcel Dekker, New York.)

Deformation of the cell lip is accomplished by bringing one, or preferably several, hardened tools or rollers against the lip at an oblique angle while the cell is rotated slowly. The lens should be held axially against the cell shoulder by external means (not shown in the figure) during the burnishing procedure to help keep it centered. If the radial fit between the lens and cell wall is close and the lens rim is accurately ground, this technique results in a well-centered subassembly. Once completed (see right view of Figure 6.4), the subassembly is essentially permanent.

This technique is most frequently used for mounting small lenses such as those for microscope or camera objectives where space constraints restrict use of separate retainers.

In some designs, a thin, narrow "washer" of resilient material such as a plastic or a thin rubber O-ring is inserted between the lens and the shoulder to soften the interface and provide some measure of sealing. Other designs may incorporate a coil spring between the lens and shoulder to offer some preload and flexibility against shock and vibration loads.[2,5]

Retaining Ring Mounts

The most frequently used technique for mounting lenses is to clamp the lens near its rim between a shoulder (or spacer in multiple component designs) and a retaining ring. The ring may be threaded loosely (Class 1 or 2 fit per ANSI Publication B1.1-1982) into the cell ID or held by screws as if it were a flange. The axial force exerted by the ring onto the lens is termed axial preload. The magnitude of this preload is determined at assembly and generally varies with temperature due to differences in thermal expansion coefficients of the materials involved. One reason for providing axial preload is to hold the lens in place under acceleration due to shock and/or vibration. The magnitude of preload, P_{ACC}, required for this purpose may be approximated by the expression:

$$P_{ACC} = WA F_S \tag{1}$$

where W is the weight of the lens, A is the maximum acceleration expected, and F_S is a safety factor (typically at least 2).

Axial preload induces axial stress into the lens and cell as discussed in the Section "Axial Stress at Single Element Interfaces". Manufacturing variations in axial dimensions of lenses and cells can be compensated with this type of mounting. It is compatible with environmental sealing with a cured-in-place elastomer or O-ring. Retaining ring designs also accommodate multiple component lens systems that are separated by spacers as discussed in Section 6.3.

Threaded Ring

Figure 6.5 illustrates a typical threaded retaining ring mount design for a biconvex lens. Contact between the lens and the mechanical parts occurs on the polished glass surfaces as recommended for precise centering of the optical axis to the mechanical axis of the cell and to minimize the need for precise edging or close tolerances on diameter of the lens.[2] This contact usually occurs slightly outside the clear aperture of the optical surface. To minimize bending of the lens, contact should occur approximately at the same height from the axis on both sides of the lens.[6] Since the spherical surface (either convex or concave) is more or less tilted with respect to the axis at the contact region due to its curvature, an axial preload applied at any point around the lens rim develops a force component directed toward the axis that tends to center the lens. When the lens is centered, these radial components balance each other and tend to hold the lens in the aligned condition. Hopkins[7] reported that a net difference in inclination of the front and back lens surfaces at the contact height of at least 17° is needed to achieve centering by means of axial preload.

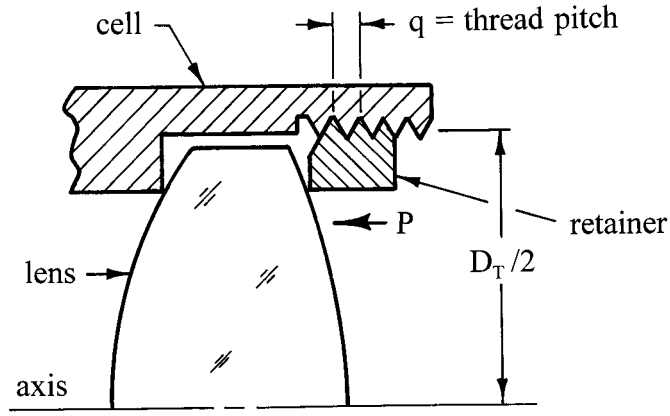

FIGURE 6.5 Typical configuration of a lens held in place by axial preload, P, from a threaded retaining ring. (From Yoder, P.R., Jr. 1993. *Opto-Mechanical Systems Design*, 2nd ed. Marcel Dekker, New York.)

The magnitude of the total preload (P) developed by a specific threaded retainer lens mount design with a specific torque (Q) applied to the ring at a fixed temperature can be estimated by the following equation:

$$P = 5Q/D_T \tag{2}$$

where D_T is the pitch diameter of the thread as shown in Figure 6.5.[2,8]

Clamping (Flange) Ring

A typical design for a lens mount involving a clamped (flange-type) retaining ring is shown in Figure 6.6. This type constraint is most frequently used with large aperture lenses where manufacture and assembly of a threaded retainer would be difficult. The retainer is usually configured with a sufficient tangential stiffness so that it does not warp significantly between the clamping bolts, thereby ensuring approximately uniform pressure against the lens surface around its rim. With preload applied symmetrically, this type of mount functions essentially like the threaded ring mount described above.

The magnitude of the preload produced by a given axial deflection of the flange can be approximated by considering it to be a perforated circular plate with outer edge fixed and uniform axially

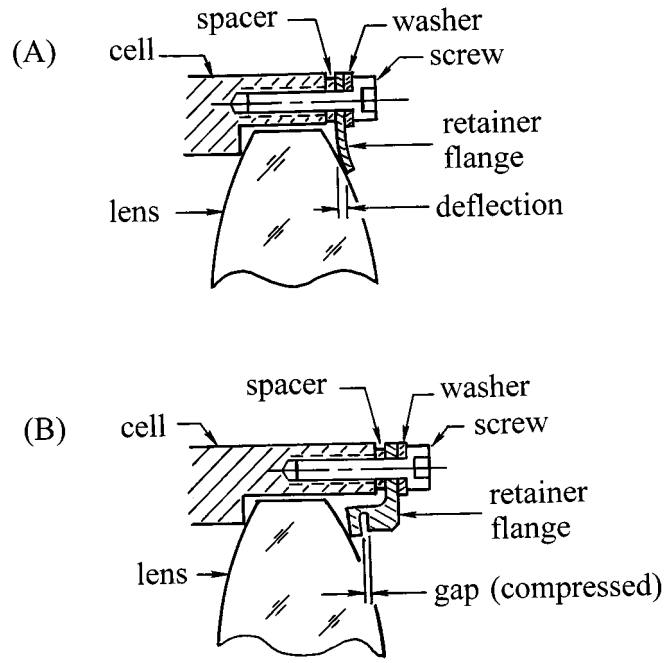

FIGURE 6.6 Typical configurations of lenses held in place by clamped flange-type retainers.

directed load applied along the inner edge to deflect that edge. Applicable equations are given by Rourk.[9] The spacer under the flange can be ground at assembly to the particular axial thickness that produces the predetermined flange deflection when firm metal-to-metal contact is achieved by tightening the clamping bolts. Variations in as-manufactured lens thicknesses, are easily accommodated with this technique. The flange material, thickness, and annular width are the prime design variables. The change in gap upon tightening the mounting screws can be measured to determine the flexure deflection in configuration (B) of Figure 6.6.

Techniques for Distributing Preload

Mounting designs using stiff flanges or retainers tend to contact the lens at the three highest points at low preload and at many points at higher preload. Stress concentrations and surface deformations may result in the latter case.[6]

Preload can be distributed more evenly with flexure designs such as shown in Figure 6.6 or 6.7. Registry for lens alignment purposes occurs at the lens-to-shoulder interface in all cases. Each type of threaded retainer provides some measure of resiliency in an attempt to distribute the force uniformly around the lens rim. In view (A), multiple flexures are built into a separate ring.[8] In view (B), an O-ring of about 70 durometer is compressed to 50 to 70% of nominal deflection.[11] In the design shown in view (C), the dimension "x" is machined at assembly to cause a predetermined amount of bending of the flexure when the retainer is firmly seated.[2] It is used with a convex surface. The configuration of view (D) serves the same function for a concave surface.

Sealing Techniques

Lenses mechanically clamped with threaded or flange-type retainers can be sealed to their cells by injecting elastomeric sealants into annular grooves machined into the retainer or cell. O-rings can be incorporated into some designs for this purpose.[10] Figure 6.8 illustrates each of these techniques. The lens should register against the cell for alignment purposes in both cases. Injected elastomeric sealant is usually inserted after all adjustments between lens and cell have been completed. Note that the elastomer must touch the lens all around its rim. If a retainer is used, it is advisable to

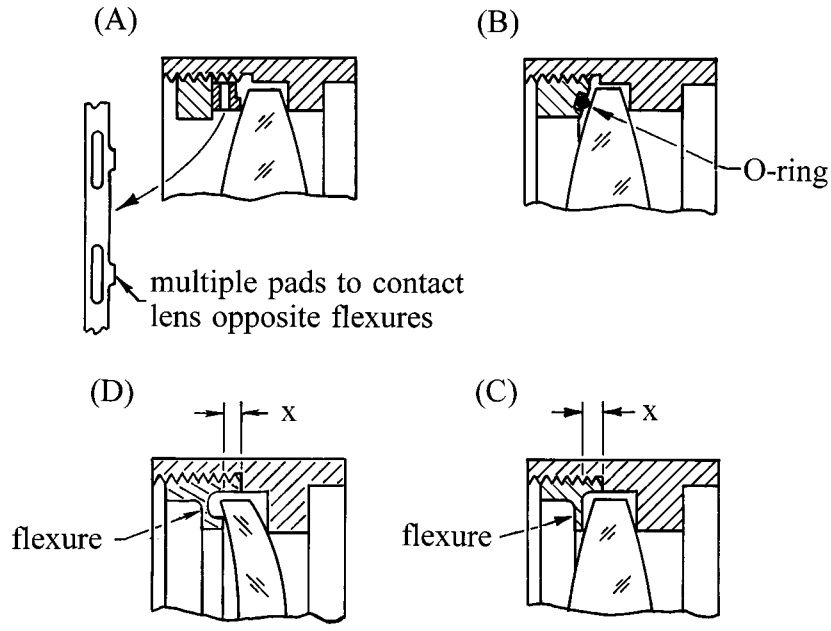

FIGURE 6.7 Some concepts for creating axially resilient interfaces between a lens and its mount to distribute preload more uniformly. (Views (A), (B), and (C) from Yoder, P.R., Jr. 1993. *Opto-Mechanical Systems Design*, 2nd ed. Marcel Dekker, New York.)

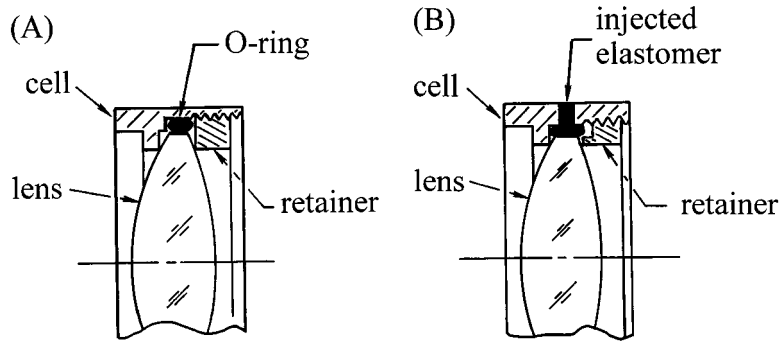

FIGURE 6.8 Typical means for sealing a lens into its cell with (A) an O-ring and (B) cured-in-place elastomer.

provide an annular airspace for the elastomer to expand into at high temperature. This is hard to do with the sealant injected after the retainer is in place. In designs with O-rings, the ring should have a durometer as large as 70 and preferably would be located around the periphery of the lens. Interfaces should be dimensioned so the ring is nominally compressed about 50 to 70% of full recommended compression at assembly. More or less compression can then take place as the temperature changes without losing sealing capability or causing undue stress.[11]

Axial Stress at Single Element Interfaces

General Considerations

The axial stress developed within the lens due to the applied axial preload depends upon the magnitude of that preload, the geometry of the interface, and the physical properties of the materials involved. The preload generally varies with temperature and this causes related changes in axial stress.

The axial stress is maximum within the narrow annular area of contact between the metal and glass. It therefore is frequently called "contact stress". The stress is generally lower at points within the lens more remotely located from the contact area.

The axial contact stress (S_A) in a lens preloaded at a height y from the axis is estimated from the following equation adapted by Yoder[2] from Roark:[9]

$$S_A = 0.798\left(K_1 p / K_2\right)^{1/2} \tag{3}$$

where K_1 depends upon the optomechanical interface design and the lens surface radius, K_2 depends upon the elastic properties of the glass and metal materials, and p is the linear preload as determined from the total preload (P) by:

$$p = P/2\pi y \tag{4}$$

The term K_1 will be discussed later in conjunction with the various interface types.

For all interface types, the term K_2 is given by:

$$K_2 = K_G + K_M = \left[\left(1-\upsilon_G^2\right)/E_G\right] + \left[\left(1-\upsilon_m^2\right)/E_M\right] \tag{5}$$

where υ_G, E_G, υ_M, and E_M are Poisson's ratio and Young's modulus values for the contacting glass and metal, respectively.

The size of the contact area depends upon the same parameters as the stress. Under light preload, the contact is essentially a "line" of length $2\pi y$. As the preload increases, the line contact widens and the resulting area is computed as $2\pi y\Delta y$ where Δy is the annular width of the elastically deformed area. The equation for Δy as adapted by Yoder[2] from Roark[9] is

$$\Delta y = 1.6\left(K_2 p / K_1\right)^{1/2} \tag{6}$$

where all terms except K_1 are as defined above.

The "Sharp Corner" Interface

The "sharp corner" interface was first defined by Delgado and Hallinan[12] as one in which the nominally 90° intersection of the machined surfaces on the metal part has been burnished in accordance with good shop practice to a radius of the order of 0.002 in. (0.05 mm). This small-radius surface contacts the glass at a height y. Figure 6.9(A) illustrates a typical design for a biconvex lens. The "hole" in the retainer referred to in the figure accepts a pin on a wrench used to tighten the retainer. A diametrical slot is frequently used for this purpose.

Hopkins[7] indicated that the machinist is more likely to achieve a smooth edge on a "sharp corner" and the chance of damage to that edge during assembly is minimized if the angle between intersecting surfaces is greater than 90°. Figure 6.9(B) shows such a design with 135° included angles as applied to a biconcave lens.

Again applying equations from Roark,[9] Yoder[2] showed that the value of K_1 in Equation 3 for any optomechanical interface is given by:

$$K_1 = \left(D_1 \pm D_2\right)/D_1 D_2 \tag{7}$$

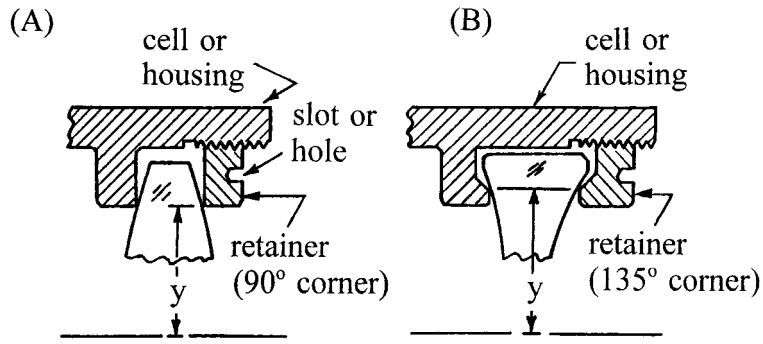

FIGURE 6.9 Schematics of "sharp corner" interfaces on (A) convex lens surfaces and (B) concave lens surfaces.

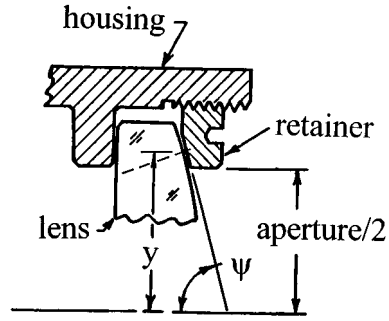

FIGURE 6.10 Schematic of a tangential interface on a convex lens surface.

where D_1 = 2(surface radius) and D_2 = 2(corner radius). The "+" sign is used for convex surfaces and the "–" sign is used for concave surfaces. K_1 is always assigned a positive sign.

In the case of the "sharp corner" interface, D_2 is typically 0.004 in. (0.1 mm).[12] For surface radii larger than about 0.2 in. (5.1 mm), D_2 can be ignored and the value of K_1 is constant at 250/in. (10/mm).[2]

The Tangential Interface

An interface design in which the lens surface contacts a conical surface in the mount is called a tangential interface. Figure 6.10 illustrates such a design. Note, this type interface is not feasible with a concave lens surface. The cone half-angle ψ is determined by the following equation:

$$\psi = 90° - \arcsin\left(y/R\right) \tag{8}$$

where R is the surface radius.

It is common practice to define the contact height y as the midpoint between the clear aperture and the edge of the polished surface. The tolerance on ψ in a given design depends primarily on the radial width of the conical annulus on the metal part and the allowable error in axial location of the lens vertex. Typically, this tolerance is about ±1°.

Since D_2 of Equation 7 is infinite for a tangential interface, the value of K_1 reduces to $1/D_1$ = 0.5/R where R is the surface radius.[2] The axial stress developed in a lens of given surface radius by a given preload with a tangential interface is smaller by a factor of $(250\ D_1)^{1/2}$ than that with a "sharp corner" interface.

The Toroidal Interface

Figure 6.11 shows toroidal (or donut-shaped) mechanical surfaces contacting convex and concave lens surfaces. Yoder[13] demonstrated that the axial stress developed in a given lens with surface radius R at given preload with a toroidal interface is essentially the same as that of the tangential interface if the cross section radii of the toroids are at least –10R for a convex lens surface and 0.5R for a concave lens surface. The corresponding values for K_1 are –0.55/R and 0.5/R for the convex and concave cases, respectively. The axial stresses developed in these lenses with these preferred toroidal radii are significantly reduced from those that would prevail with "sharp corner" interfaces.

Achievement of accurate cross-sectional radii on toroidal interfaces is not essential since stresses vary slowly with these parameters in the regions of the preferred values.[13] Tolerances of +100% are common. Figure 6.12 shows typical concepts for toroidal spacers to be used between concave or convex lens surfaces.

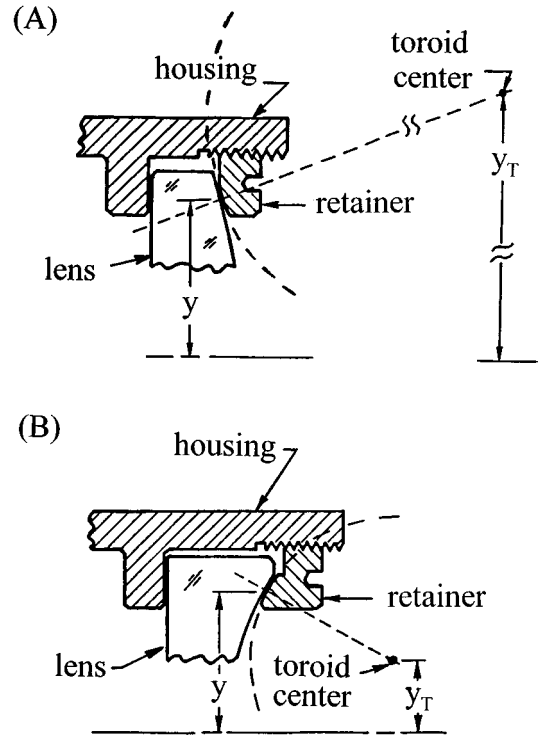

FIGURE 6.11 Schematics of toroidal interfaces on (A) a convex lens surface and (B) a concave lens surface.

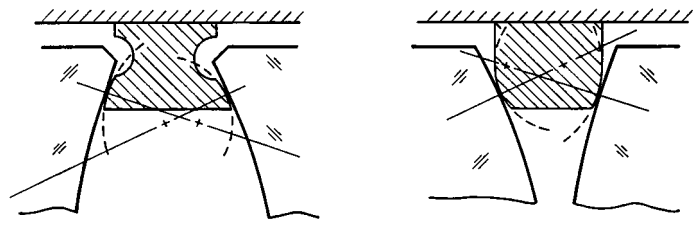

FIGURE 6.12 Schematics of spacers with toroidal interfaces. (From Yoder, P.R., Jr. 1991. *Optomechanics and Dimensional Stability, SPIE Proc. Vol. 1533*, Paquin, R.A. and Vukobratovich, D., eds., p. 2.)

The Spherical Interface

Figure 6.13 illustrates typical spherical contact lens-to-cell interfaces for convex and concave surfaces. Such designs have the advantage of distributing axial preloads over large annular areas and hence are virtually stress-free. If the surfaces match closely in both curvature and optical figure, the contact stress equals the total preload divided by the annular area of contact. As indicated by the dashed lines in both views, the design must provide access for lapping in order to produce accurate spherical interfaces on the mount. Surface matching requires very careful manufacture and increases cost. For this reason, the spherical interface is not frequently used.

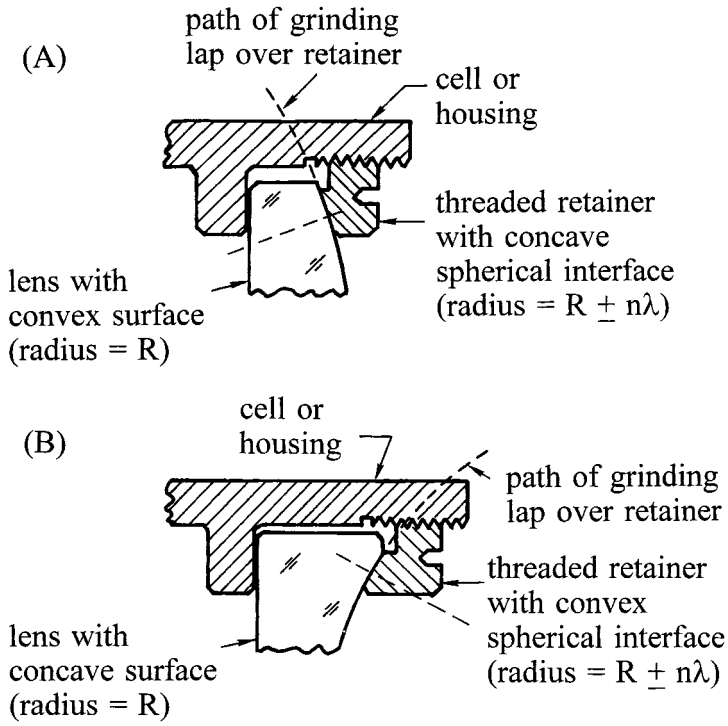

FIGURE 6.13 Schematics of spherical interfaces on (A) a convex lens surface and (B) a concave lens surface.

Flat and Step Bevel Interfaces

In Figure 6.14 a lens mount configuration involving flat bevels on concave and convex surfaces is shown. To facilitate alignment, a flat bevel should be accurately perpendicular to the optical axis of the lens. If used on a convex surface, a step should be ground into the rim of that surface. If intimate contact with the mount occurs over a flat bevel uniformly around the rim of the lens, the contact stress at the interface equals the total preload divided by the annular area of contact.

If flat bevels are used on both sides of a lens having optical power in both surfaces, as frequently is the case with biconcave lenses, both should be perpendicular to the lens optical axis. If this is not the case, it is impossible to accurately align the optical axis to the mechanical axis of the subassembly. Self-centering by applying axial preload also is impossible with flat bevels applied to both lens surfaces. A preferred interface for a concave surface is the toroidal one illustrated in Figure 6.11(B).

Parametric Comparisons of Interface Types

Figure 6.15 shows the nature of the variation of axial stress with radius of the contacting corner for a particular design having a given convex lens surface radius and a given mechanical preload.

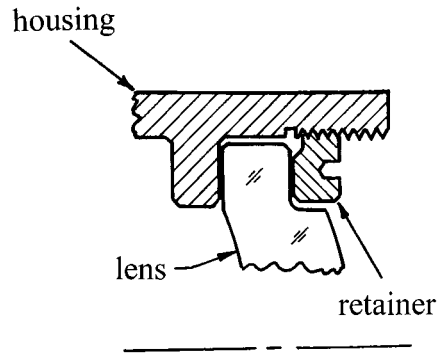

FIGURE 6.14 Schematics of flat bevel interfaces on (left) a concave lens surface and (right) a convex lens surface.

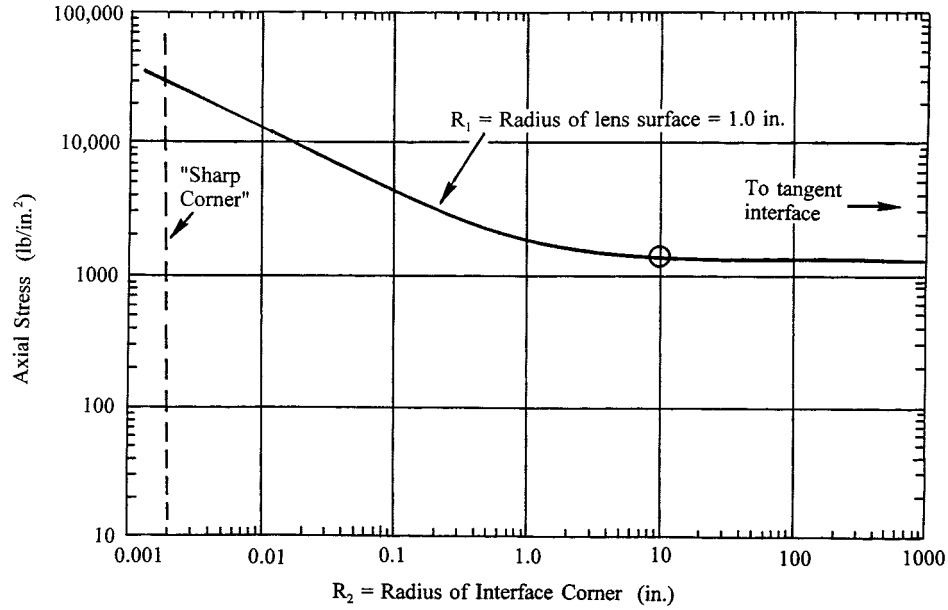

FIGURE 6.15 Variation of axial stress in a typical lens at constant preload as the radius of the mechanical surface contacting its convex surface is changed. (From Yoder, P.R., Jr. 1993. *Optomechanical Design, SPIE Proc. Vol. 1998*, Vukobratovich, D., Yoder, P.R., Jr., and Genberg, V., eds., p. 8.)

Both stress and corner radius are plotted logarithmically to cover large ranges of variability. At the left is the short corner radius characteristic of the "sharp corner" interface, while at the right, the tangential interface case is approached asymptotically. Between these extremes are an infinite number of toroidal interface designs. The "preferred" toroidal radius (equal to –10R) for which the stress is within 5% of the value for a tangential interface is indicated by the circle.[13]

Figure 6.16 shows a similar relationship for a concave lens surface example. The "sharp corner" case is again at the left. As the toroidal radius increases toward the matching radius (spherical interface) limit, the stress decreases. The circle represents the "preferred" toroidal radius of 0.5R for which the stress approximates that which would prevail at the same preload on a convex surface of the same radius using a –10R toroidal interface.[13]

The last two figures show conclusively that the axial contact stress is always significantly higher with a "sharp corner" interface than with any other type. It has been recommended that whenever

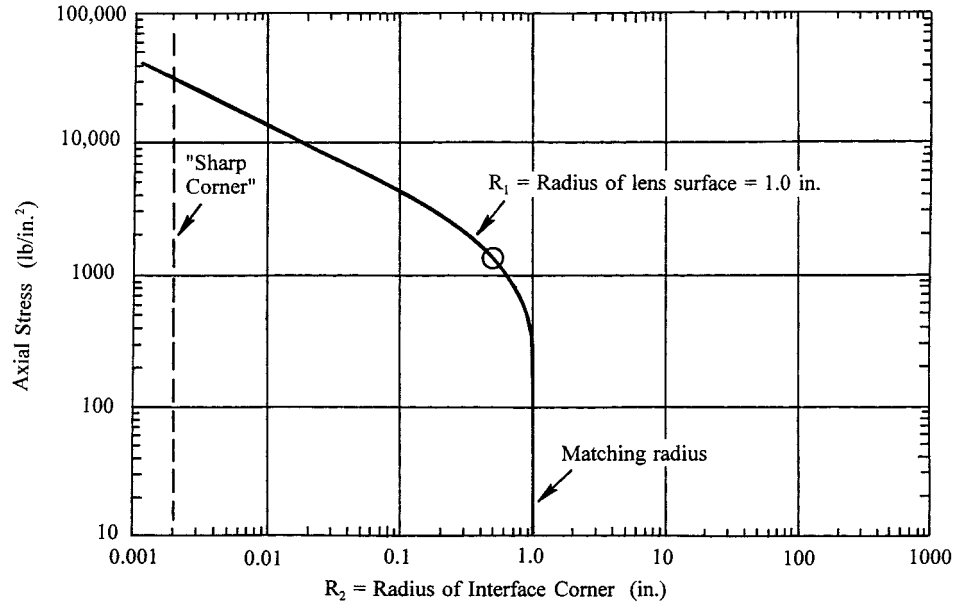

FIGURE 6.16 Variation of axial stress in a typical lens at constant preload as the radius of the mechanical surface contacting its concave surface is changed. (From Yoder, P.R., Jr. 1993. *Optomechanical Design, SPIE Proc. Vol. 1998*, Vukobratovich, D., Yoder, P.R., Jr., and Genberg, V., eds., p. 8.)

slightly higher manufacturing cost can be tolerated, tangential interfaces be used on all convex lens surfaces and toroidal interfaces of radius approximately 0.5R be used on all concave surfaces.[13]

Stress Variation with Surface Radius

Figures 6.17 and 6.18 show graphically how the axial stress varies as the surface radius is changed by successive factors of 10 for convex and concave surface cases, respectively. The preload is held constant. The stress is seen to be independent of surface radius or its algebraic sign for a "sharp corner" interface (left side of each graph). The greatest changes occur for long-radii toroids on either type surface, for the "tangential interface on a convex surface", and the "matching radii on a concave surface" cases. It has been shown[13] that, for the toroids indicated by the circles on each curve (toroid radius = –10R for convex and 0.5R for concave), if the surface radius changes from R_1 to R_2 with all other parameters unchanged, the corresponding stress changes by $(R_1/R_2)^{1/2}$. Hence, for the 10:1 increases in surface radius depicted in Figures 6.17 and 6.18, the stress decreases by a factor of $0.1^{1/2} = 0.316$.

Stress Variation with Preload

If the total preload, P, on a lens with any type interface and any surface radius increases from P_1 to P_2 while all other parameters remain fixed, the resulting axial contact stress changes by a factor of $(P_2/P_1)^{1/2}$. A tenfold increase in preload therefore increases the stress by a factor of 3.162.[13]

Effects of Changing Materials

The first (K_G) and second (K_M) terms of Equation 5 apply independently to the two materials in contact at the lens-to-mount interface.[14] Although lenses are commonly made of glass, crystals, or plastic, considerations here are limited to optical glass materials.

Walker[15] selected 62 basic types of optical glass offered by various manufacturers that "span the most common range of index and dispersion and have the most desirable characteristics in terms of price, bubble content, staining characteristics and resistance to adverse environmental conditions." The factor K_G of Equation 5 has been calculated for each of the 68 Schott varieties included

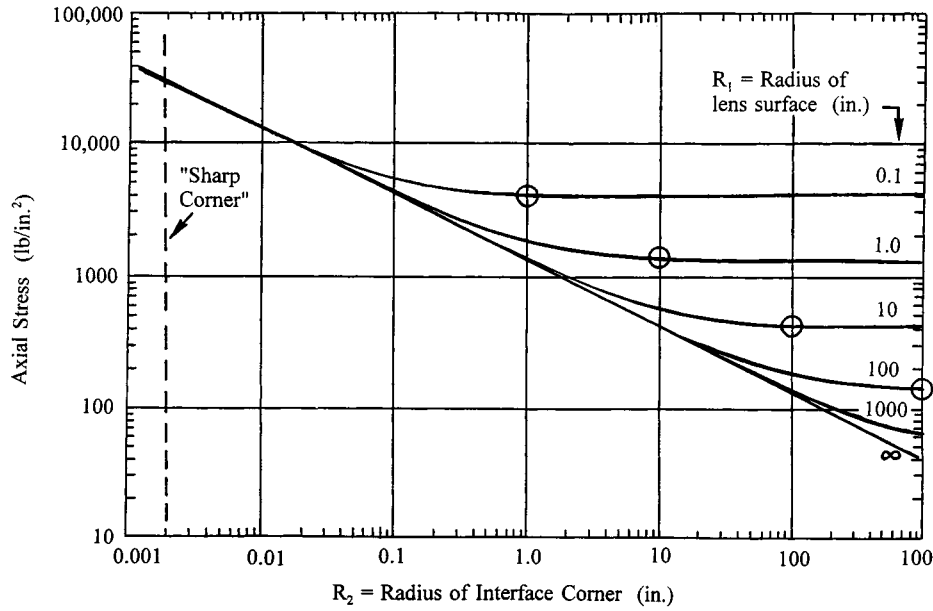

FIGURE 6.17 Variations of axial stress in a family of typical lenses at constant preload as the radius of the mechanical surface contacting a convex surface and the radius of that surface are changed. (From Yoder, P.R., Jr. 1991. *Optomechanics and Dimensional Stability, SPIE Proc. Vol. 1533*, Paquin, R.A. and Vukobratovich, D., eds., p. 2.)

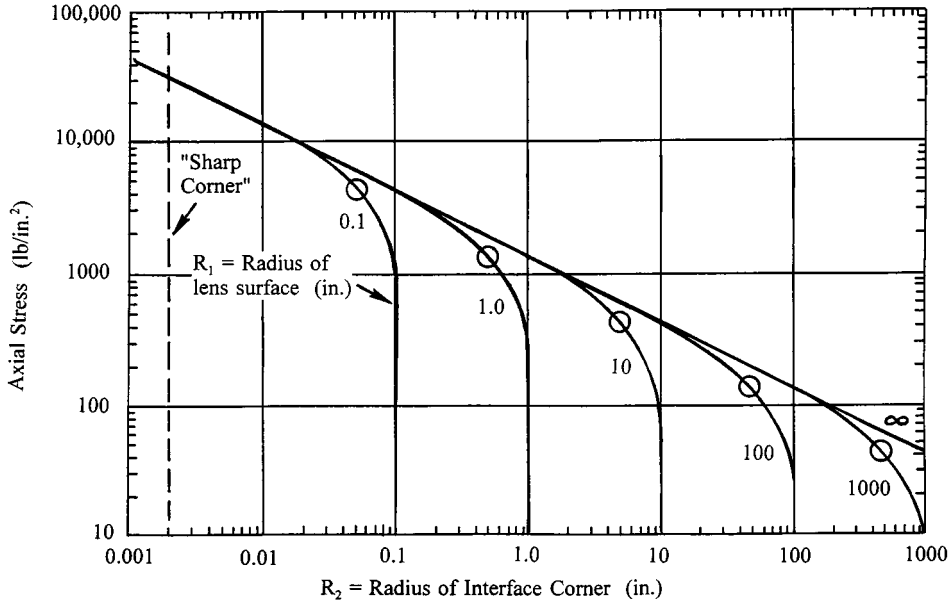

FIGURE 6.18 Variations of axial stress in a family of typical lenses at constant preload as the radius of the mechanical surface contacting a concave surface and the radius of that surface are changed. (From Yoder, P.R., Jr. 1991. *Optomechanics and Dimensional Stability, SPIE Proc. Vol. 1533*, Paquin, R.A. and Vukobratovich, D., eds., p. 2.)

in Walker's list. Figure 6.19 shows, in bar-graph form, how the magnitude of K_G varies for this family. The sequence is by increasing glass-type designation and hence by increasing index of refraction. There is no apparent correlation between K_G and index of refraction. The glasses with

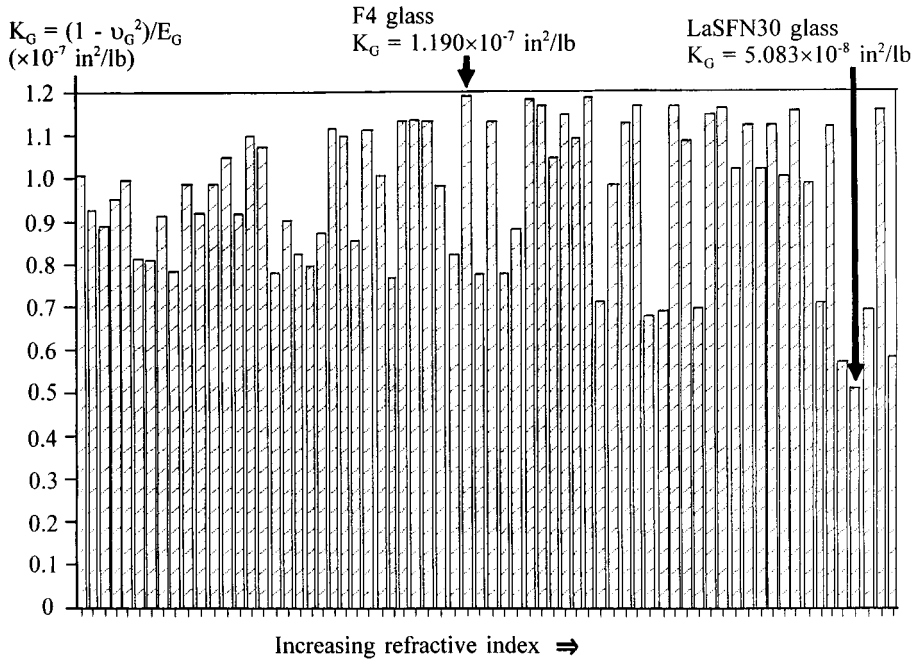

FIGURE 6.19 Variation of magnitude of K_G for 68 Schott glasses selected by Walker.[15] The left-to-right sequence is by increasing glass type code and, hence, by refractive index. (From Yoder, P.R., Jr. 1993. *Opto-mechanical Design, SPIE Proc. Vol. 1998*, Vukobratovich, D., Yoder, P.R., Jr., and Genberg, V., eds., p. 8.)

Table 6.1 Selected Mechanical Properties of the Schott Glasses Included in Walker's[14] List of Preferred Glass Types that have the Lowest and Highest Value for K_G

Glass Name	Glass Type	$K_G = (1 - \upsilon_G^2)/E_G$ in.^{2}/lb (m^2/N)	Young's Modulus E_G lb/in.^{2} (N/m^2)	Poisson's Ratio υ_G	Thermal Expansion Coefficient α_G/°F (/°C)
F4	617366	1.190×10^{-7}	7.98×10^{6}	0.225	4.6×10^{-6}
		(1.726×10^{-11})	(5.50×10^{10})		(8.3×10^{-6})
LaSFN30	803464	5.083×10^{-8}	1.80×10^{7}	0.293	3.4×10^{-6}
		(7.372×10^{-12})	(1.24×10^{11})		(6.2×10^{-6})

Adapted from Yoder, P.R., Jr. 1991. *Optomechanics and Dimensional Stability, SPIE Proc. Vol. 1533*, Paquin, R.A. and Vukobratovich, D., eds., p. 2.

the highest (F4) and lowest (LaSFN30) values of K_G are indicated in the figure by arrows. The ratio of K_G values for these extreme glasses is 2.34. Table 6.1 gives the pertinent mechanical properties of these two glasses. Properties data were obtained from the Schott catalog.[16]

Table 6.2 lists key mechanical properties of six types of metals selected for consideration here. K_M was calculated from Equation 5 and varies from 2.366×10^{-8} in.^{2}/lb (for beryllium) to 1.350×10^{-7} in.^{2}/lb (for magnesium). The ratio of these extreme values is 5.70. Figure 6.20 shows graphically how K_M varies for these metals.

It should be noted that low values for either K_G or K_M tend to increase lens stress since these factors appear in the denominator of Equation 3.

Yoder[14] analyzed combinations of the metals from Table 6.2 with the two glasses of Table 6.1 in a typical glass-to-metal design with preload and interface-type constant. Figure 6.21 shows plots of variations of axial stress with material type. The vertical scale is normalized to the stress level of a BK7 lens in an aluminum mount (triangle). The horizontal scale is Young's modulus for the metals. The horizontal spacings of the vertical dashed lines representing the selected metals give a sense of the variation of this important parameter from one metal to another. The two curved

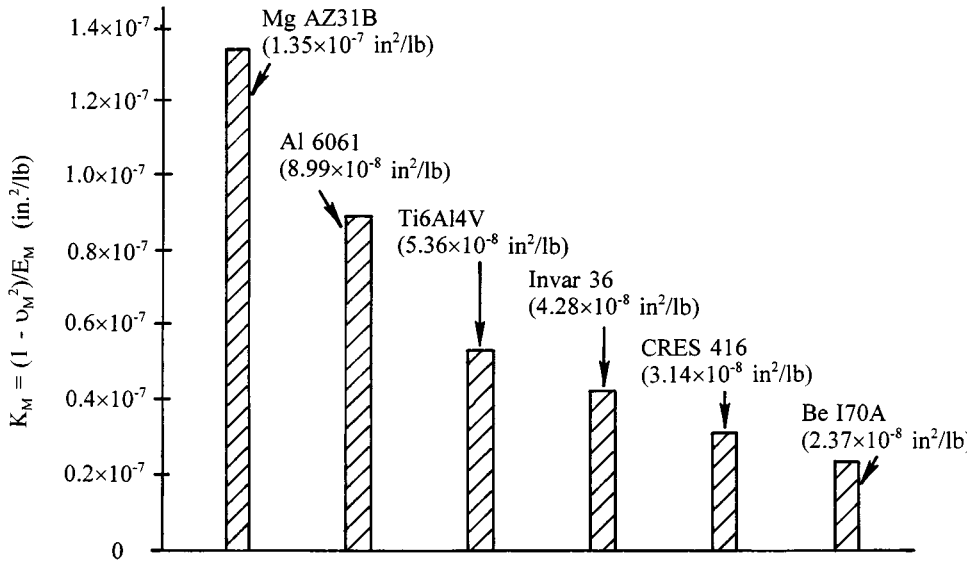

FIGURE 6.20 Variation of K_M for six metals typically used in lens mounts in optical instruments. (From Yoder, P.R., Jr. 1993. *Optomechanical Design, SPIE Proc. Vol. 1998*, Vukobratovich, D., Yoder, P.R., Jr., and Genberg, V., eds., p. 8.)

Table 6.2 Selected Mechanical Properties of Some Metals Used in Lens Mounts. Sequence is by Increasing K_M

Metal Type	$K_M = (1 - \upsilon_M^{2)}/E_M$ in.²/lb (m²/N)	Young's Modulus E_M lb/in.² (N/m²)	Poisson's Ratio υ_M	Thermal Expansion Coefficient α_M °F (/°C)
Be I70A	2.366×10^{-8}	4.2×10^{7}	0.080	1.6×10^{-5}
	(3.438×10^{-12})	(2.89×10^{11})		(1.13×10^{-5})
CRES 416	3.138×10^{-8}	2.90×10^{7}	0.300	5.5×10^{-6}
	(4.55×10^{-12})	(2.00×10^{11})		(9.9×10^{-6})
Invar 36	4.28×10^{-8}	2.14×10^{7}	0.290	7.0×10^{-7}
	(6.231×10^{-12})	(1.47×10^{11})		(1.26×10^{-6})
Ti6Al4V	5.36×10^{-8}	1.65×10^{7}	0.340	4.9×10^{-6}
	(7.758×10^{-12})	(1.14×10^{11})		(8.8×10^{-6})
Al 6061	8.988×10^{-8}	9.9×10^{6}	0.332	1.3×10^{-5}
	(1.305×10^{-11})	(6.82×10^{10})		(2.36×10^{-5})
Mg AZ31B	1.350×10^{-7}	6.50×10^{6}	0.350	1.4×10^{-5}
	(1.959×10^{-11})	(4.48×10^{10})		(2.52×10^{-5})

Adapted from Yoder, P.R., Jr. 1991. *Optomechanics and Dimensional Stability, SPIE Proc. Vol. 1533*, Paquin, R.A. and Vukobratovich, D., eds., p. 2.

lines connect discrete points representing particular combinations of glasses and metals and are not really continuous functions. The fact that the curves diverge toward the right indicates the greater significance of differing glass characteristic K_G for the stiffer metals having smaller K_M values.

Rate of Change of Preload with Temperature

If, as is usually the case, the lens and mount materials have dissimilar thermal expansion coefficients; temperature changes, ΔT, cause changes in total axial preload, P, exerted onto the lens. The following equation[2] quantifies this relationship:

$$\Delta P = K_3 \Delta T \tag{9}$$

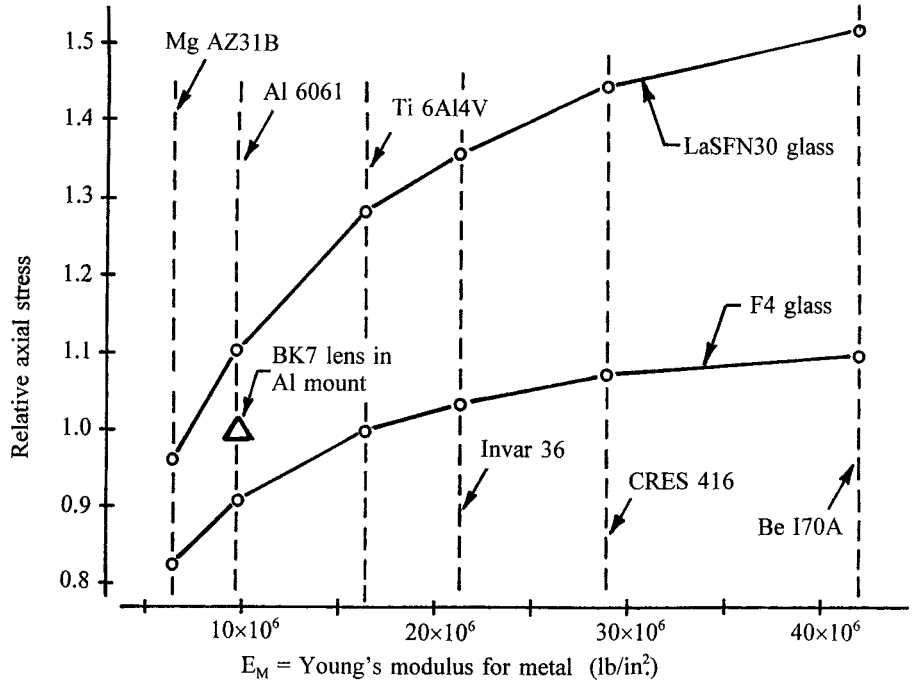

FIGURE 6.21 Variations of normalized axial stress in lenses made of two types of glass when mounted in different metals. (From Yoder, P.R., Jr. 1993. *Optomechanical Design, SPIE Proc. Vol. 1998*, Vukobratovich, D., Yoder, P.R., Jr., and Genberg, V., eds., p. 8.)

where

$$K_3 = \frac{-E_G A_G E_M A_M (\alpha_M - \alpha_G)}{E_G A_G + 2E_M A_M} \tag{10}$$

Here, υ_G, E_G, υ_M, and E_M are as defined above and α_M and α_G are thermal expansion coefficients of the two materials. The terms A_G and A_M represent cross-sectional areas of the annular stressed regions within the lens and within the mount. These geometric parameters are shown in Figures 6.22 and 6.23.

Equations for A_G and A_M follow:

$$\text{If } (2y + t_E) < D_G, \text{ then } A_G = 2\pi y t_E \tag{11}$$

$$\text{If } (2y + t_E) \geq D_G, \text{ then } A_G = (\pi/4)(D_G - t_E + 2y)(D_G + t_E - 2y) \tag{12}$$

$$A_M = 2\pi t_C \left[(D_M/2) + (t_C/2)\right] \tag{13}$$

where t_E is the edge thickness of the lens at the contact height y, t_C is the radial wall thickness of the mount at the lens rim, D_M is the ID of the mount at the lens rim, and D_G is the OD of the lens.

The relationship between preload change and temperature change (Equation 9) is linear for any combination of lens and mount materials. The factor K_3 is the slope of this line. A negative value for K_3 means that a drop in temperature (negative ΔT) increases preload. As shown by Yoder,[14] it depends upon geometry of the design as well as the material properties. With lens and mount

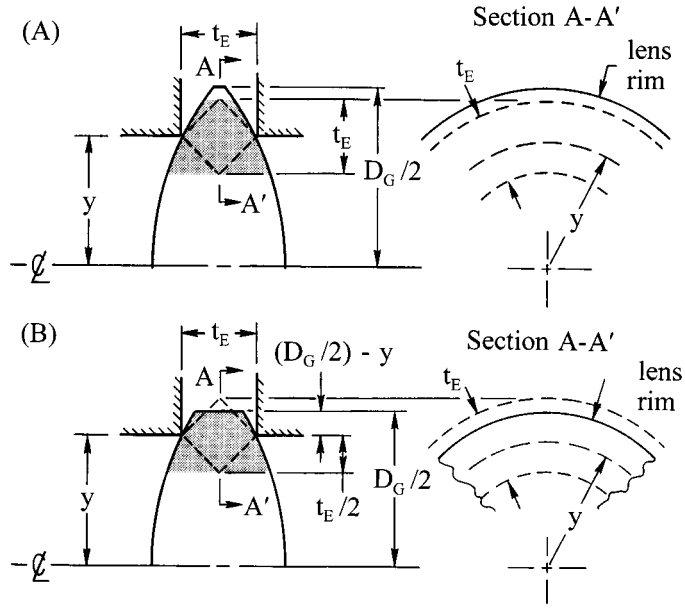

FIGURE 6.22 Geometric relationships used to determine the cross-sectional areas of the stressed regions within a clamped lens, (A) when the region lies within the lens rim and (B) when the stressed region is truncated by the rim. (From Yoder, P.R., Jr. 1992. *Optomechanical Design, SPIE Proc. CR43*, Yoder, P.R., Jr., ed., p. 305.)

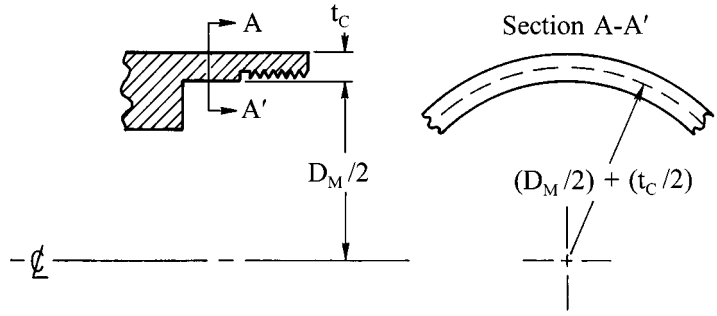

FIGURE 6.23 Geometric relationships used to determine the cross-sectional area of the axially stressed lens cell. (From Yoder, P.R., Jr. 1992. *Optomechanical Design, SPIE Proc. CR43*, Yoder, P.R., Jr., ed., p. 305.)

materials having a small difference between their expansion coefficients, the values of K_3 and the significance of postassembly temperature changes would be expected to be smaller than if this difference is large.

Growth of Axial Clearance at Increased Temperature

If α_M exceeds α_G (as is usually the case), the metal of the mount will expand more than the glass component as the temperature rises. Any axial preload existing at assembly temperature, T_A (typically 20°C [68°F]), will then be reduced. If the temperature rises sufficiently, that preload will disappear and, if not otherwise constrained (as by an elastomeric sealant), the optic is free to move within the mount due to external forces. In nearly all applications, some changes in position and orientation of the lens within small axial and radial gaps created by differential expansion are allowable. The mount should maintain contact with the lens to some elevated temperature, T_C, defined so that *further* temperature increase to the specified maximum survival temperature would not cause the axial gap between mount and lens to exceed the design tolerance.

The axial gap developed between the cell and the lens as temperature rises above T_C can be approximated as:

$$Gap_A = (\alpha_M - \alpha_G)(t_E)(T_{MAX} - T_C) \tag{14}$$

where all terms are as defined above. If Gap_A is equated to the tolerable value, a unique value for T_C of a given design can be calculated. Knowing the rate of change of preload with temperature, K_3, from Equations 10 through 13, the required preload at assembly can be adjusted so that it is just reduced to zero at T_C. Defining the temperature change from T_A to T_C as $-\Delta T$, Equation 9 can then be used to estimate the assembly preload.[2]

Preload and Stress at Low Temperature

In designs where α_M exceeds α_G, the magnitude of the assembly preload is increased whenever the temperature drops below T_A. The total preload at any low temperature, T, can be estimated from Equation 9 by setting ΔT equal to $(T - T_C)$. The axial contact stress created by that preload can then be calculated with the aid of Equations 4 and 3. When T equals the specified minimum survival temperature, T_{MIN}, the stress should not exceed the tolerable compressive value for the glass.

Bending Stress Due to Preload

If the annular areas of contact between the mount and the lens are not directly opposite (i.e., at the same height from the axis on both sides), a bending moment is created within the glass. This moment causes the lens to bend so one side becomes more convex and the other side becomes more concave. The surface that becomes more convex is placed in tension while the other surface is compressed. Since glass breaks much more easily in tension than in compression, especially if the surface is damaged by scratches or has subsurface cracks, catastrophic failure may occur.

An analytical model based upon a thin plane-parallel plate and using an equation from Roark[9] applies also to simple lenses.[6] This is illustrated in Figure 6.24. The tensile stress due to bending of the lens is given by:

$$S_T = \frac{3P}{2\pi m t_E^{\,2}}\left[0.5(m-1) + (m+1)\ln\frac{y_2}{y_1} - (m-1)\frac{y_1^{\,2}}{2y_2^{\,2}}\right] \tag{15}$$

where P = total applied preload

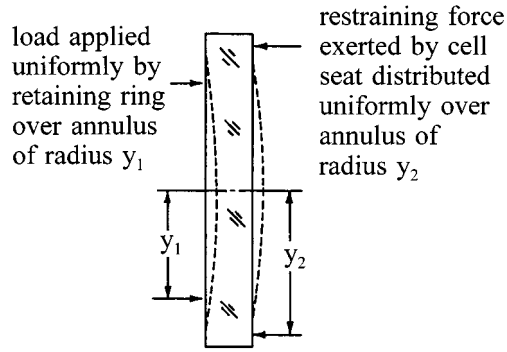

FIGURE 6.24 Simplified representation of optical element (plane-parallel plate) bent by clamping between interfaces at different heights. (From Yoder, P.R., Jr. 1993. *Opto-Mechanical Systems Design*, 2nd ed. Marcel Dekker, New York.)

m = 1/Poisson's ratio for the element
t_E = element edge thickness
y_i = contact height on surface "i"

To decrease the probability of breakage from this cause, the contact heights should be made equal within a few percent. Increasing the lens thickness also tends to reduce this danger.

Axial Stress at Multiple Element Interfaces

In the above section ("Axial Stress at Single Element Interfaces"), techniques for estimating axial contact stresses in single element lenses were discussed. That theory was extended by Yoder[17] to include multiple lens designs such as cemented doublets and optomechanical designs with spacers or equivalent cell shoulders between separated lenses. The applicable equations and the procedures for use thereof are summarized here for the convenience of the reader.

The Cemented Doublet

Figure 6.25 shows a typical cemented doublet clamped between a cell shoulder and a threaded retainer. For simplicity, the contact heights are assumed to be the same at both interfaces. The stressed region in the glass is the annulus of radial width ($t_{E1} + t_{E2}$) as indicated by the dashed diamond. Equation 11 or 12, as appropriate, is used to calculate A_G as if the lens were a homogeneous single element. Equation 13 is used to determine A_M. These areas, pertinent component dimensions and the applicable material properties, can then be substituted into the following equation to determine the temperature sensitivity factor K_3:

$$K_3 = \frac{-(\alpha_M - \alpha_{G1})t_{E1} - (\alpha_M - \alpha_{G2})t_{E2}}{\dfrac{2t_{E1}}{E_{G1}A_G} + \dfrac{2t_{E2}}{E_{G2}A_G} + \dfrac{(t_{E1} + t_{E2})}{E_M A_M}} \tag{16}$$

Given the total preload, P, at assembly, the linear preload, p, at any temperature can be calculated using Equations 9 and 4. Note that this preload is the same at both the first and third surfaces of the lens. Then the applicable value of K_2 at either of these surfaces can be estimated by Equation 5 using the material properties prevailing at that interface. Finally, knowing the type of interface and surface radius at each surface, the value for K_1 can be calculated and the contact stress at that surface can be estimated through use of Equation 3. In general, the stresses at the two surfaces will

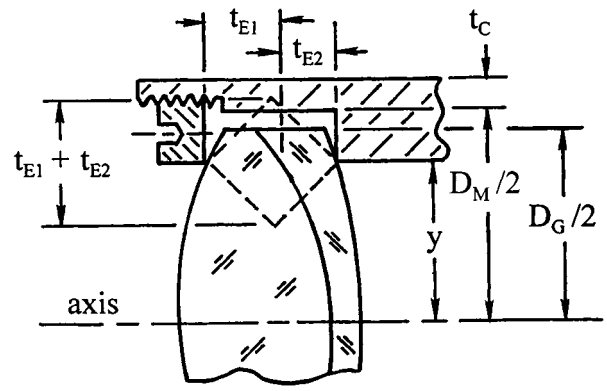

FIGURE 6.25 Schematic of a cemented doublet clamped axially in a cell. The stressed region in the lens is indicated by the dashed diamond. (From Yoder, P.R., Jr. 1994. *Current Developments in Optical Design and Engineering, SPIE Proc. Vol. 2263*, Fischer, R.E. and Smith, W.J., eds.)

differ because the glasses have different elastic and thermal properties. The interface types and surface radii also may differ, thereby affecting the values of K_1.

If the temperature rises sufficiently to dissipate assembly preload, an axial gap between the doublet and the mount develops for additional temperature increases in accordance with the following equation:

$$\Delta x = \left[\left(\alpha_M - \alpha_{G1}\right) t_{E1} + \left(\alpha_M - \alpha_{G2}\right) t_{E2}\right] \Delta T \tag{17}$$

The Air-Spaced Doublet

A simple mounting for an air-spaced doublet comprising two unequal diameter elements with differing edge thicknesses is illustrated in Figure 6.26. The spacer material may be different from that of the cell. The glasses also may be different. The contact heights at both surfaces of a given lens are assumed equal and the cell wall thickness is assumed to be constant in this example. If the contact heights at the individual lenses are the same, a cylindrical spacer with parallel OD and ID is used. In the figure, the spacer has a cylindrical OD and a tapered ID. The preload, P, is the same at all lens surfaces.

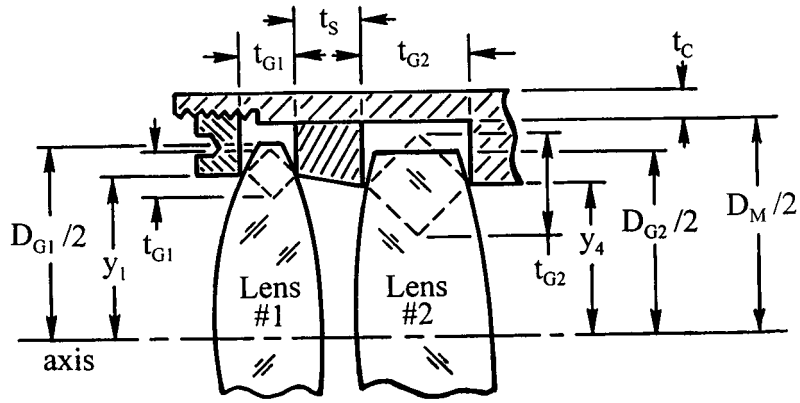

FIGURE 6.26 Schematic representation of two air-spaced lens elements clamped axially in a cell. The stressed regions in the lenses are indicated by the dashed diamonds. (From Yoder, P.R., Jr. 1994. *Current Developments in Optical Design and Engineering, SPIE Proc. Vol. 2263*, Fischer, R.E. and Smith, W.J., eds.)

The following equations give the applicable values of K_3 and the axial gap, Δx, for temperature increases above that for which the preload reaches zero:

$$K_3 = \frac{-(\alpha_M - \alpha_{G1}) t_{G1} - (\alpha_M - \alpha_S) t_S - (\alpha_M - \alpha_{G2}) t_{G2}}{\dfrac{2t_{G1}}{E_{G1}A_{G1}} + \dfrac{t_S}{E_S A_S} + \dfrac{2t_{G2}}{E_{G2}A_{G2}} + \dfrac{(t_{G1} + t_S + t_{G2})}{E_M A_M}} \tag{18}$$

$$\Delta x = \left[\left(\alpha_M - \alpha_{G1}\right) t_{G1} + (\alpha_M - \alpha_S) t_S + \left(\alpha_M - \alpha_{G2}\right) t_{G2}\right] \Delta T \tag{19}$$

where all terms are as defined above.

Sectional views of two types of simple lens spacers are shown in Figure 6.27. Both are solid cylinders fitting closely into the ID of the lens cell. The version shown in view (B) has a tapered ID to accommodate different heights of contact with the lenses. It also shows tangential interfaces. Equations 20 through 25 allow the annular areas, A_S, to be calculated for each of these spacers.

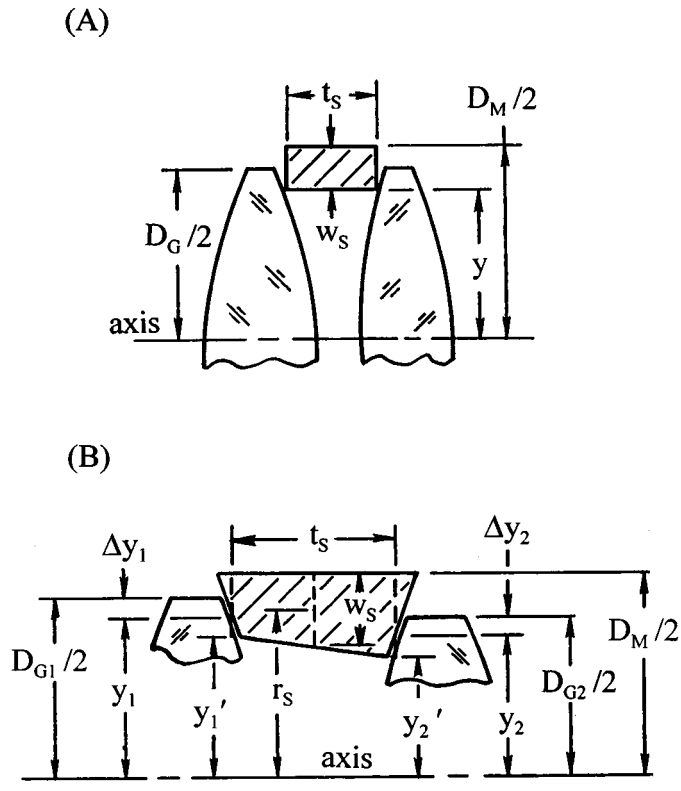

FIGURE 6.27 Sectional views of two types of lens spacers, (A) solid cylindrical-type with "sharp corner" interfaces at equal heights and (B) solid tapered-type with tangential interfaces at different heights. (From Yoder, P.R., Jr. 1994. *Current Developments in Optical Design and Engineering, SPIE Proc. Vol. 2263*, Fischer, R.E. and Smith, W.J., eds.)

For spacer version (A):

$$w_S = \left(D_M/2\right) - y \tag{20}$$

For spacer version (B), the wall thickness of the tapered spacer is taken as its average annular thickness calculated as follows:

$$\Delta y_i = \left(D_{Gi}/2\right) - y_i \tag{21}$$

$$y_i' = y_i - \Delta y_i \tag{22}$$

$$w_S = \left(D_M/2\right) - \left[\left(y_1' + y_2'\right)/2\right] \tag{23}$$

In both cases:

$$r_S = \left(D_M/2\right) - \left(w_S/2\right) \tag{24}$$

$$A_S = 2\pi r_S w_S \tag{25}$$

By following the same sequence of calculations as described for the cemented doublet, the contact stresses at the four air–glass interfaces can be estimated.

General Formulation for Multiple Elements

Figure 6.28 provides a schematic example for stress estimation in a more complex multiple element design. Here, different cemented doublets, "A" and "B", are separated by a spacer of uniform annular thickness, t_C, in a cell with constant ID adjacent to the lens rims. A single retainer applies axial preload. The interfaces are all "sharp corners". The cross-sectional areas of the lenses are A_A and A_B, while those for the cell wall and spacer are A_M and A_S. These areas are calculated with the aid of Equations 11 or 12, 13, 20, 24, and 25.

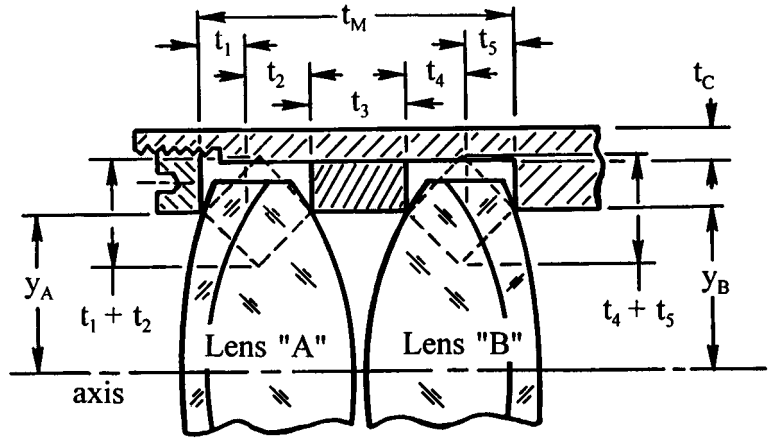

FIGURE 6.28 Schematic of two air-spaced cemented doublet lenses clamped axially in a cell. The stressed regions in the lenses are indicated by the dashed diamonds. (From Yoder, P.R., Jr. 1994. *Current Developments in Optical Design and Engineering, SPIE Proc. Vol. 2263*, Fischer, R.E. and Smith, W.J., eds.)

The applicable equation for K_3 of this design is

$$K_3 = \frac{-(\alpha_M - \alpha_1)t_1 - (\alpha_M - \alpha_2)t_2 - (\alpha_M - \alpha_3)t_3 - (\alpha_M - \alpha_4)t_4 - (\alpha_M - \alpha_5)t_5}{\frac{2t_1}{E_1A_A} + \frac{2t_2}{E_2A_A} + \frac{2t_3}{E_3A_3} + \frac{2t_4}{E_4A_B} + \frac{2t_5}{E_5A_B} + \frac{t_M}{E_MA_M}} \tag{26}$$

This equation has, in its numerator, the sum of negative terms comprising the axial thicknesses of each lens element and of the spacer at the applicable height of contact multiplied by the pertinent differences in thermal expansion coefficients for those parts relative to that of the cell. In the denominator is found the sum of reciprocals of the spring constants for each part of the subassembly. The first five terms in the denominator represent parts in compression and the last three terms represent segments of the cell wall in tension.

The calculations leading to estimation of the axial contact stress at each interface involve first the application of Equations 9 and 4 to determine the linear preload, p, for all air–glass interfaces at any temperature given the total applied preload, P. Then the applicable value of K_2 at each interface is calculated by Equation 5 using the material properties prevailing at that interface. Finally, knowing the type of interface and surface radius at each surface, the value for K_1 can be calculated and the contact stress at each surface can be estimated through use of Equation 3.

The axial gap, Δx, for temperature increases above that for which the preload reaches zero can be calculated for this design by the following equation:

$$\Delta x = \left[(\alpha_M - \alpha_1)\, t_1 + (\alpha_M - \alpha_2)\, t_2 + (\alpha_M - \alpha_3)\, t_3 + (\alpha_M - \alpha_4)\, t_4 + (\alpha_M - \alpha_5)\, t_5\right] \Delta T \tag{27}$$

With understanding of the general formats of Equations 26 and 27, their extension to even more complex multiple element designs is facilitated. The procedure explained earlier can then be applied to determine the axial contact stress for those designs at any temperature.

Radial Stress

Radial Stress in Single Elements

In all the designs considered above, radial clearance was assumed to exist between the lens and the mount. In some designs, this clearance is the minimum allowing assembly so, at some reduced temperature, the metal touches the rim of the optic and, at still lower temperatures, a radially-directed force and resultant radial stress develops. The magnitude of this stress, S_R, for a given temperature drop, ΔT, can be estimated as[2]

$$S_R = K_4 K_5 \Delta T \tag{28}$$

Here:

$$K_4 = \left(\alpha_M - \alpha_G\right) \Big/ \left[\left(1/E_G\right) + \left(D_G/2E_M t_C\right)\right] \tag{29}$$

and

$$K_5 = 1 - \left\{\left(2\,\Delta r\right) \Big/ \left[D_G\, \Delta T \left(\alpha_M - \alpha_G\right)\right]\right\} \tag{30}$$

where

D_G = lens OD
t_c = mount wall thickness outside the rim of the lens
Δr = radial clearance

If Δr exceeds $D_G\, \Delta T(\alpha_M - \alpha_G)/2$, the lens will not be constrained by the cell ID and radial stress will not develop within the temperature range ΔT due to rim contact.

Tangential Hoop Stress within the Cell Wall

As another consequence of differential contraction of the cell relative to the lens, stress is built up within the metal in accordance with the equation:

$$S_M = S_R D_G / 2t_c \tag{31}$$

where all terms are as defined above.[6] With this expression, one can determine if the cell is strong enough to withstand the force exerted upon the lens without exceeding its elastic limit. If the yield strength of the metal exceeds S_M, a safety factor exists.

Radial Stress within Multiple Elements

In designs involving multiple separated lenses, the radial stress in any element is determined on an individual basis as discussed in the above section "Radial Stress within the Cell Wall". Cemented doublets of uniform OD made of glasses with different coefficients of thermal expansion are usually treated by considering only the element with greatest difference in α as compared to that of the mount. Doublets made up of elements with significantly unequal ODs are treated by considering only the largest element.

Radial Forces Resulting from Axial Preload

Axial preload, P, applied symmetrically to a curved lens surface of radius, R, at some height, y, from the axis produces an inwardly directed radial force component at all contact points. This force tends to compress radially that portion of the glass within the contact zone. The magnitude of this radial force equals (P sin θ cos θ), where θ is the angular inclination of the surface normal at the contact height relative to the axial direction. For designs with θ = arc tan (y/R) no larger than about 6°, this radial force is no larger than P/10. It reaches P/3 at about 21°. Only with large axial preloads and/or short surface radii does this factor become a significant contributor to radial stress.

Growth of Radial Clearance at Increased Temperature

The increase in radial clearance, ΔGap_R, between the optic and the mount due to a temperature increase of ΔT from that at assembly can be estimated by the equation:

$$\Delta Gap_R = \left(\alpha_M - \alpha_G\right) D_G \, \Delta T / 2 \tag{32}$$

where all terms are as previously defined.

Elastomeric Suspension Interfaces

A Typical Configuration

Figure 6.29 shows a typical design for a lens suspended by an annular ring of resilient elastomeric material (typically epoxy, urethane, or room temperature vulcanizing rubber) within a cell.[6] One side of the elastomer ring is unconstrained so as to allow the material to deform under compression or tension due to temperature changes and maintain a constant volume.[18] Registration of one optical surface against a machined surface of the cell helps align the lens.[3] Centration can be established prior to curing and maintained throughout the cure cycle with shims or external fixturing.

First-Order Thermal Effects

If the resilient layer has a particular radial thickness, the assembly will be athermal to first-order approximation in the radial direction. Stress buildup within the optomechanical components due to differential expansion or contraction is then resisted. This thickness is

$$t_E = \left(D_G/2\right)\left(\alpha_M - \alpha_G\right)/\left(\alpha_E - \alpha_M\right) \tag{33}$$

where α_E is the thermal expansion coefficient of the elastomer and all other terms are as defined above.

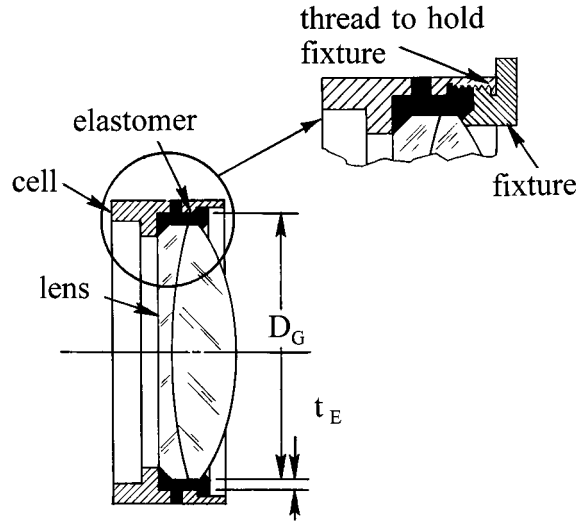

FIGURE 6.29 Schematic of a lens component supported within a cell by an annular layer of cured-in-place elastomer. The detail view shows one means for retaining the injected elastomer during cure. (From Yoder, P.R., Jr. 1993. *Opto-Mechanical Systems Design*, 2nd ed. Marcel Dekker, New York.)

Gravity and Acceleration Effects

Valente and Richard[19] reported an analytical technique for estimating the decentration, Δ, of a lens mounted in a ring of elastomer when subjected to radial gravitational loading. Their method was extended[20] to include more general radial acceleration forces resulting in the following equation:

$$\Delta = AWt_E \Big/ \left[\pi Rd \left\{ \left[E_E \Big/ \left(1 - \upsilon_E^2 \right) \right] + E_S \right\} \right] \tag{34}$$

where

A = acceleration factor
W = weight of optical component
t_E = thickness of elastomer layer
R = optical component OD/2
d = optical component thickness
E_E = Young's modulus of elastomer
E_S = Shear modulus of elastomer
and ν_E = Poisson's ratio of elastomer

The decentrations of modest-sized optics corresponding to normal gravity loading are generally quite small, but tend to grow under shock and vibration loading. Fortunately, the resilient material will tend to restore the lens to its unstressed location and orientation when the acceleration loading dissipates.

6.3 Lens Assemblies

"Drop-In" Assembly

Designs in which the lens(es) and the features of the mount that interface therewith are manufactured to specified dimensions within specified tolerances and assembled without further machining and with a minimum of adjustment are called "drop-in" assemblies. Low cost, ease of assembly,

and simple maintenance are prime criteria for these designs. Typically, relative apertures are f/4.5 or slower and performance requirements are not particularly high.

An example is shown in Figure 6.30. This is a fixed-focus eyepiece for a military telescope.[2] Both lenses (identical doublets back to back) and a spacer fit into the ID of the cell with typically 0.003 in. (0.075 mm) diametric clearance. The threaded retainer holds these parts in place. "Sharp corner" interfaces are used throughout. Accuracy of centration depends primarily upon the accuracy of lens edging and the ability of the axial preload to "squeeze out" differences in edge thickness before the rims of the lenses touch the cell ID. The axial air space between the lenses depends upon the spacer dimensions which are typically held to design values within 0.010 in. (0.25 mm).

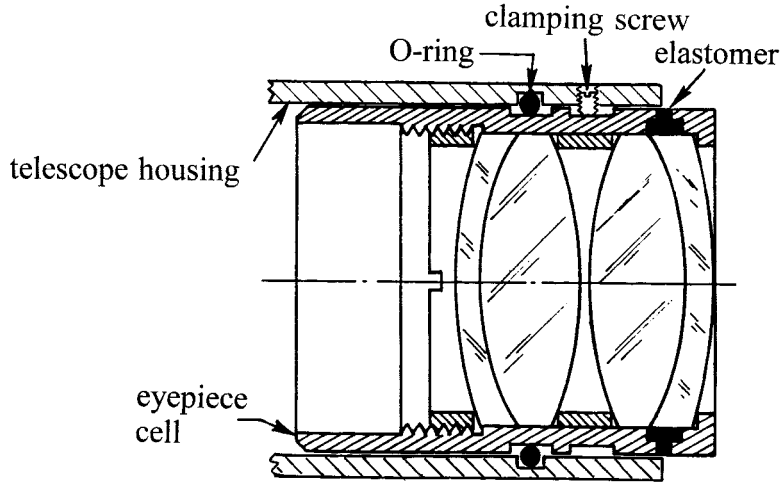

FIGURE 6.30 Example of a fixed-focus eyepiece for a military telescope with lenses and mechanical parts premachined and assembly by the "drop-in" technique. (Adapted from Yoder, P.R., Jr. 1993. *Optical Systems Engineering III, SPIE Proc. Vol. 389*, Taylor, W.H., ed., pp. 2–11.)

Lens assemblies for many commercial applications traditionally follow the "drop-in" design concept. Most involve high volume production and many are intended for assembly by "pick and place" robots. Thorough tolerancing guided by knowledge of normal optical and mechanical shop practices is essential since parts are usually selected from stock at random, and few, if any, adjustments at assembly are feasible.[1] It is expected that a small percentage of the end items will not meet performance requirements. Those that fail are usually discarded — that action being more cost effective than troubleshooting and fixing the problem.

An example of a commercial lens assembly is shown in Figure 6.31. This is an objective for large-screen projection television.[21] The three lenses are injection-molded polymethyl methacrylate. The molded plastic mount is constructed as two symmetrical half-cylinders that are joined longitudinally with adhesive, tape, and/or self-tapping screws after insertion of the lenses. Shoulders that locate the lenses axially are molded in place as are radially oriented mounting pads that center the lens rims. Molded-in pressure tabs are designed to flex slightly as the lenses are inserted so as to constrain the lenses even with minor axial thickness variations.

"Lathe" Assembly

A "lathe-assembled" lens is one in which the lens seats in the mount are custom machined on a lathe or similar machine to fit closely to the measured ODs of a specific lens or specific set of lenses.[2] Axial position of each seat is usually determined during this operation. For this to be successful, the lenses should be precision edged to a high degree of roundness. The tolerances on lens ODs can be relatively loose if sufficient material is provided at the corresponding seat IDs to

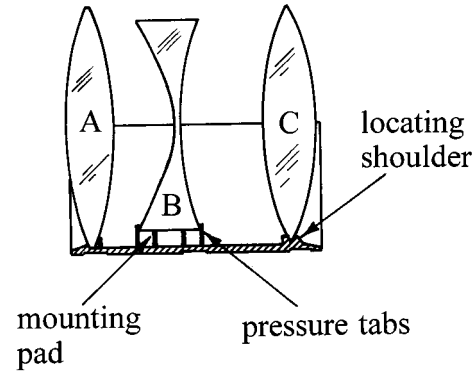

FIGURE 6.31 Optomechanical schematic of a plastic triplet mounted in a plastic mount. (From Betinsky and Welham. 1979. *Optical Systems Engineering, SPIE Proc. Vol. 193*, Yoder, P.R., Jr., ed., p. 78.)

ensure significant material removal during the fitting process. Radial clearances between lens and mount of 0.0002 in. (5.1 μm) are common, while clearances as small as 50×10^{-6} in. (1.3 μm) are feasible. With such small clearances, these lens mountings are frequently referred to as "hard mounts".

An example of the measurement/machining sequence is illustrated in Figure 6.32. View (A) shows the complete optical subassembly comprising an air-spaced doublet in a cell. Required measurements of the lenses are indicated in view (B). Surface radii also are known from test plate or interferometric measurement during manufacture. The mechanical surfaces designated by letters "A" through "E" are machined to suit this specific set of lens measurements and to position the lenses axially and radially within specified tolerances. Machining of surface "D" which provides a tangential interface for lens no. 1 is an iterative process with trial insertions of the lens and measurement of its vertex location relative to flange surface "B" to ensure achievement of the specified 57.150 mm dimension within the 10-μm tolerance. The spacer thickness also is machined iteratively with trial assembly and measurement of overall axial thickness to ensure meeting the design tolerance on this dimension.

This technique is often used in the assembly of lenses for high performance aerial reconnaissance and space science payloads.[6,22,23] For example, Figure 6.33 shows a 24-in. (61-cm) focal length, f/3.5 aerial camera objective lens designed for this method of assembly.[6] The titanium barrel is made in two parts so a shutter and iris can be inserted between lenses 5 and 6 following optical alignment. The machining of lens seats to fit measured lens ODs and to provide proper air spaces begins with the smaller diameter components and progresses toward the larger ones. Each lens is held with its own retainer so no spacers are required. The lenses are fitted into the front and back barrel components in single lathe setups to maximize centration. These optomechanical subassemblies are mechanically piloted together so their mechanical (and optical) axes coincide. An O-ring is used to seal this interface with metal-to-metal contact between the flanges. Tangent contacts are used as the convex surface interfaces. Flat bevels on concave surfaces are made with accurate perpendicularity to the lens' optical axes to facilitate centration. Because of space constraints between lenses 2–3 and 3–4, deep step recesses are ground into the rims to provide space for the retainers. Injected elastomer rings (not shown) seal lenses 1, 5, 6, and 7 to the barrel and all internal air spaces (interconnected) are purged with dry nitrogen to minimize moisture condensation at low temperatures.

Extreme care is required when inserting lenses with small radial clearances to prevent damage. As shown in Figure 6.34, the rims of thick lenses are sometimes edged spherical to minimize the risk of jamming during assembly.[22] The centers of curvature of these rims are located within close tolerances at the optical axis of the respective lenses to maximize centration accuracy. The lens

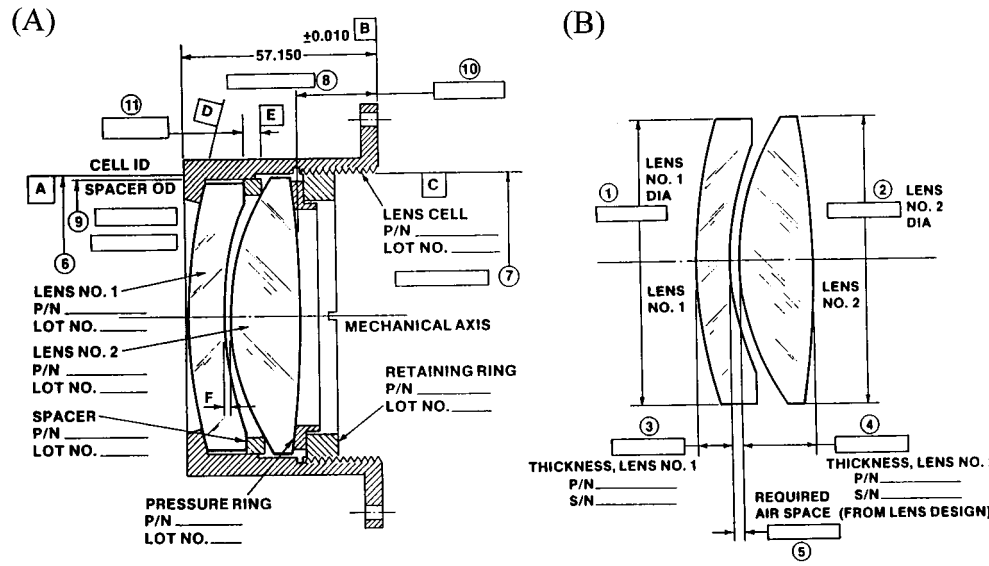

FIGURE 6.32 (A) Example of an optomechanical lens subassembly custom machined by the "lathe assembly" technique to fit a specific set of lens dimensions per (B). (From Yoder, P.R., Jr. 1993. *Optical Systems Engineering III, SPIE Proc. Vol. 389*, Taylor, W.H., ed., pp. 2–11.)

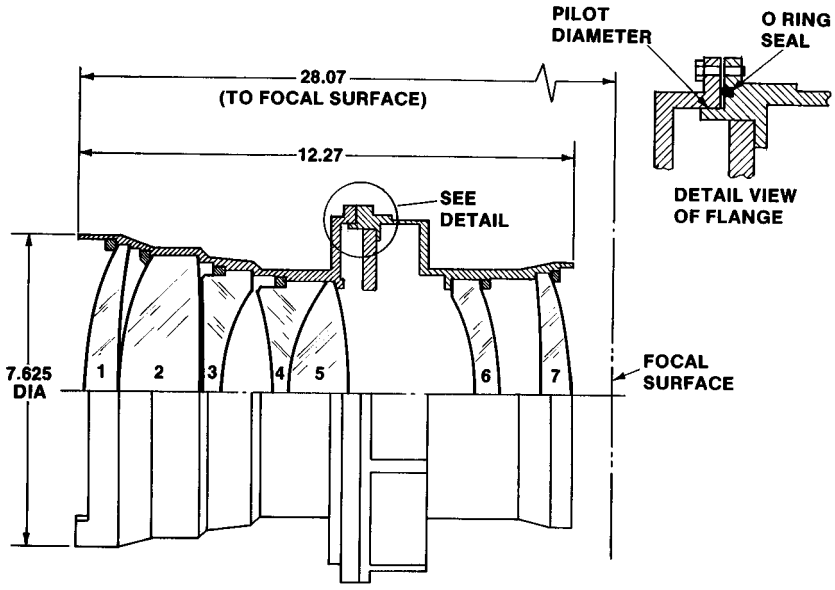

FIGURE 6.33 Sectional view of a 24-in. (61-cm) focal length, f/3.5 aerial camera objective lens designed for the lathe assembly method of assembly. (From Bayar, M. 1981. *Opt. Eng.*, 20, 181.)

assembly shown in this figure is a 9-in. (23-cm) focal length, f/1.5 objective with coaxial laser channel designed for a military night vision periscope application.[22,24]

Vukobratovich[11] described a technique for custom fitting shims between the lens rim and cell ID that essentially achieves a hard mounting with very small radial clearance or, in some cases, radial compression of the shims. Full contact around the lens rim is provided in some designs, while, in others three shorter shims are inserted symmetrically to give more kinematic support. To lock the latter shim segments in place, adhesive can be inserted through radial holes in the cell

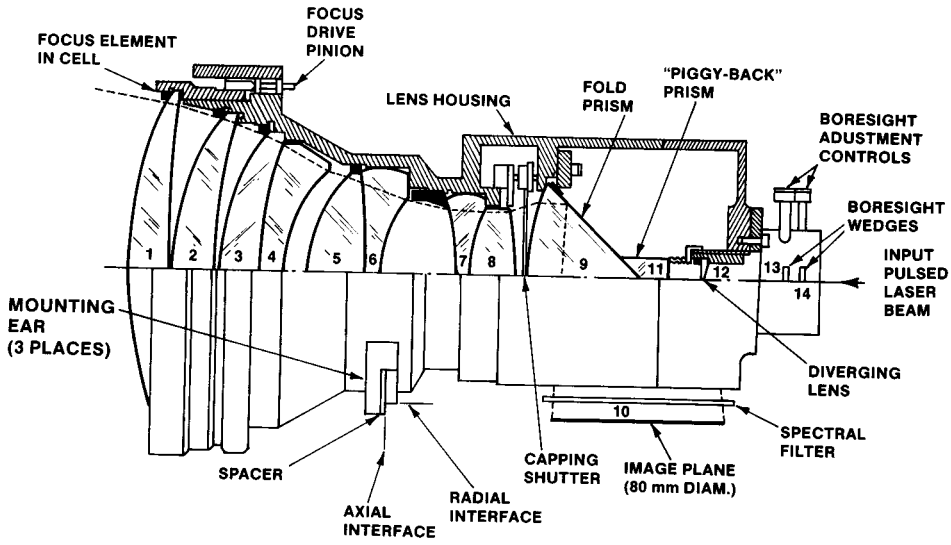

FIGURE 6.34 Sectional view of a lens assembly featuring several lenses with spherical rims assembled with small radial clearance by the "lathe assembly" technique. Shaded components are retainers. (From Yoder, P.R., Jr. 1986. *Contemporary Optical Instrument Design, Fabrication, Assembly and Testing, SPIE Proc. Vol. 656*, Beckmann, L.H.J.F., Briers, J.D., and Yoder, P.R., Jr., eds., p. 225.)

and shim walls. The segmented shim technique has been found especially useful in mounting large diameter lenses.[23]

Subcell Assembly

Optomechanical subassemblies with the lenses mounted and aligned precisely within individual subcells and those subcells inserted in sequence into precisely machined IDs of outer barrels have been described by several authors.[2,6,7,10,25,26] One recent design is illustrated in Figure 6.35.[27] The lenses of this low-distortion, telecentric projection lens were aligned within their respective stainless steel cells to tolerances as small as 0.0005-in. (12.7-μm) decentration, 0.0001-in. (2.5-μm) edge thickness runout due to wedge, and 0.0001-in. (2.5-μm) surface edge runout due to tilt. They then were potted in place with 0.015-in. (0.381-mm)-thick annular rings of 3M 2216 epoxy adhesive injected through radial holes in the subcells to secure the lenses in place. The subcell thicknesses were machined such that the air spaces between lenses were within design tolerances without adjustment. After curing, the subcells were inserted into the stainless steel barrel and secured with retainers.

Vukobratovich described an alternate technique for mounting the lenses within the subcells. Here, each lens is burnished into a subcell and then the outer surfaces of that cell machined concentric with the lens' optical axis and to proper OD for insertion along with similarly machined subcells into a barrel. In other designs, the prealigned subcells were press-fitted with radial mechanical interference into the barrel.[11,28]

Modular Assembly

Optical instrument design, assembly, and maintenance are all simplified if groups of related optical and mechanical components are constructed as prealigned and interchangeable modules. In some cases, the individual modules are nonmaintainable and repair of the instrument is accomplished by replacement of defective modules; sometimes without subsequent system alignment.

A classic example of this type design is shown in Figure 6.36. This military 7×50 binocular has prealigned and parfocalized objective and eyepiece assemblies as well as left and right housings with prealigned Porro-type erecting prisms.[2,29,30] Manufacture of such subassemblies is somewhat

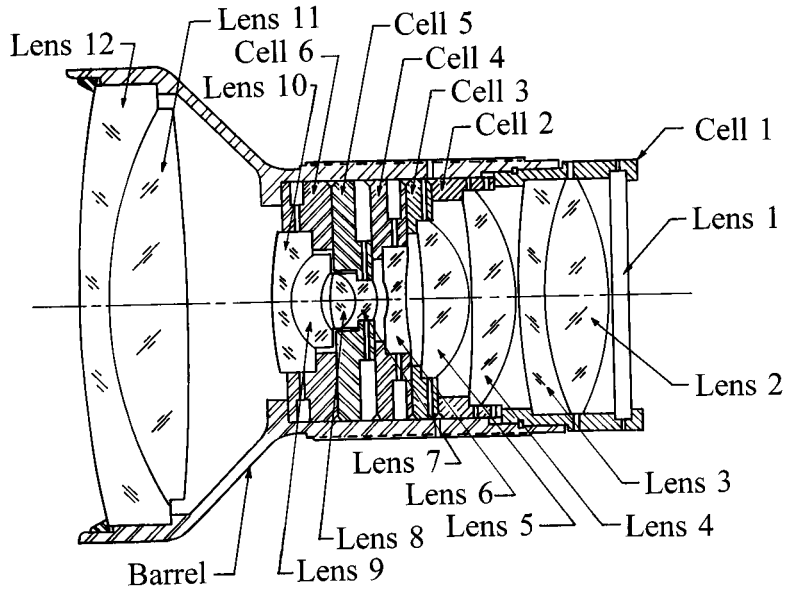

FIGURE 6.35 Sectional view of a lens system comprising several lenses mounted in and aligned to individual subcells that all fit closely within the ID of an external barrel. (Adapted from Fischer, R.E. 1991. *Optomechanics and Dimensional Stability, SPIE Proc. Vol. 1533*, Paquin, R.A. and Vukobratovich, D., eds., p. 27.)

more complex than for the equivalent nonmodular subassemblies due to the requirement for complete interchangeability. In some cases, adjustments are made within the module during assembly, while in other cases, mounting surfaces are machined to specific orientations and/or locations with respect to optical axes and focal planes. Achievement of performance goals is greatly facilitated by the design and fabrication of optomechanical fixtures specifically intended for manufacture and alignment of the modules.[30]

Many photographic and video camera lenses, microscope objectives, and telescope eyepieces are optomechanical modules. Lenses of different focal lengths, relative apertures, and physical sizes have identical mounting features so they can be installed on different instruments. In the photographic application, a variety of lenses can be interchanged on a single camera body or moved from one camera to another of similar type. These lens modules are parfocalized so their calibrated infinity focal planes automatically coincide with the camera's film plane. In some cases, adapters are available to allow lenses from one manufacturer to interface correctly with cameras made by another manufacturer.

Use of advanced injection molding techniques allows complex optomechanical subassemblies to be fabricated from plastic materials in modular form. Figure 6.37 shows such a module designed for use in an automatic coin-changer mechanism.[31] It comprises two acrylic lens elements (one aspheric) molded integral with a mechanical housing having prealigned mounting provisions and interfaces for attaching two detectors. When manufactured in large quantities, this type module is inexpensive. Since it requires no adjustments, it is easy to install and virtually maintenance free.

Many instrument designs utilize single-point diamond machining fabrication techniques to create interchangeable optomechanical modules involving precisely located and contoured reflecting surfaces. This topic is considered in Section 6.5 ("Single-Point Diamond-Turned Mirrors and Mounts"). The methods and machines described there are, in some cases, also applicable to fabricating mounts for lenses.

Elastomeric Assembly

The basic techniques for elastomeric mounting of lenses has been described in Section 6.2 ("Elastomeric Suspension Interfaces"). The advantages of resilient mounting, thermal isolation, ease of

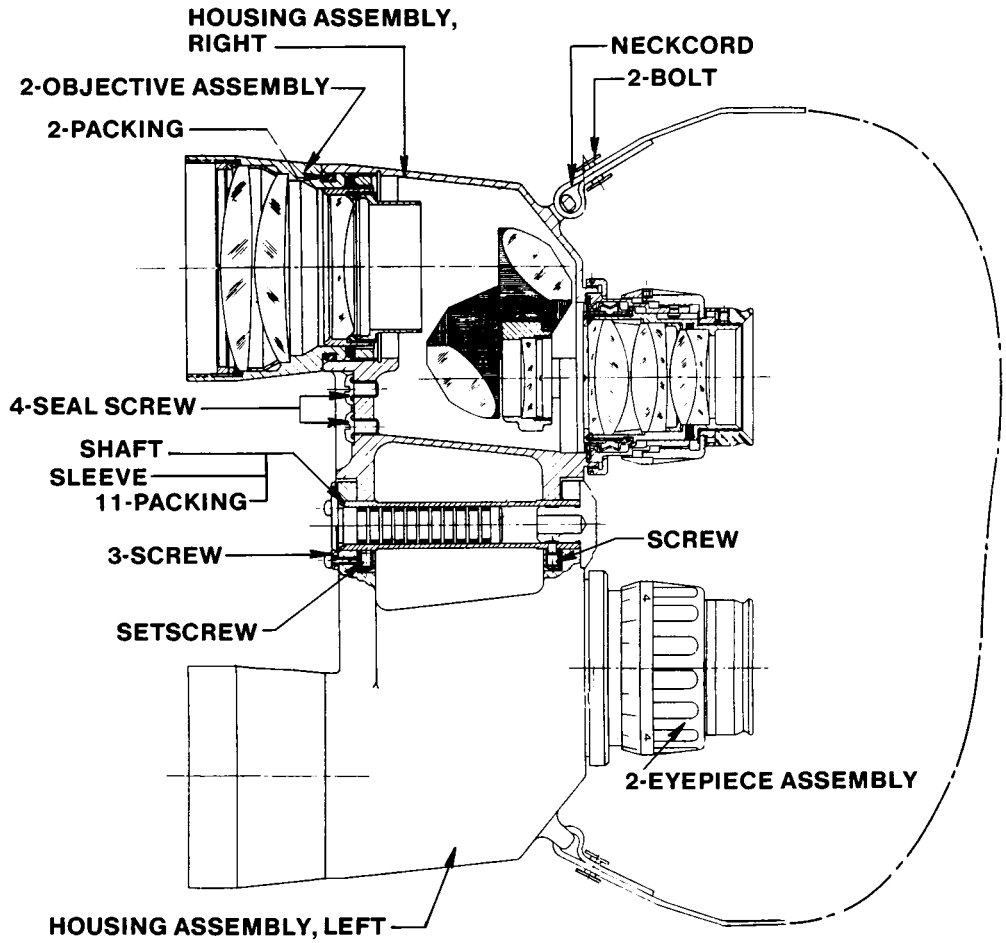

FIGURE 6.36 Sectional view of a military 7 × 50 binocular featuring interchangeable modular objective, eyepiece, and prism housing assemblies. (From Yoder, P.R., Jr. 1993. *Opto-Mechanical Systems Design*, 2nd ed. Marcel Dekker, New York.)

assembly, and inherent sealing can also be achieved in multiple element optical subassemblies. For example, Figure 6.38 shows an aerial camera objective lens in which all optical elements are suspended in rings of elastomeric material.[6] Sufficient radial clearances are provided at each lens seat so that the lenses can be centered and squared-on with respect to pilot diameters and mounting flanges on the barrel halves. Usually these features of the barrels are prealigned to the axis of rotation of a precision spindle so errors in lens alignment can be detected during rotation. In this particular design, the lenses are clamped by threaded retainers after alignment and then the elastomer is injected through several radial holes in the barrel walls to fill the annular space between the lens rim and the cell ID.

In this type design, the thickness of the resilient layer is frequently determined from Equation 33 so the assembly is approximately athermalized in the radial direction. The design is not, however, athermalized in the axial direction since the length of the elastomer layer essentially equals the edge thickness of the lens as well as the applicable length of barrel wall. Since the elastomer is here completely encapsulated and it tends to maintain constant volume with temperature change,[18] the lenses may be stressed at extreme temperatures.

The last mentioned problem can be avoided if, as shown in Figure 6.29, at least one surface of the elastomer ring is not constrained, but is free to deform (i.e., indent or bulge) with temperature changes.

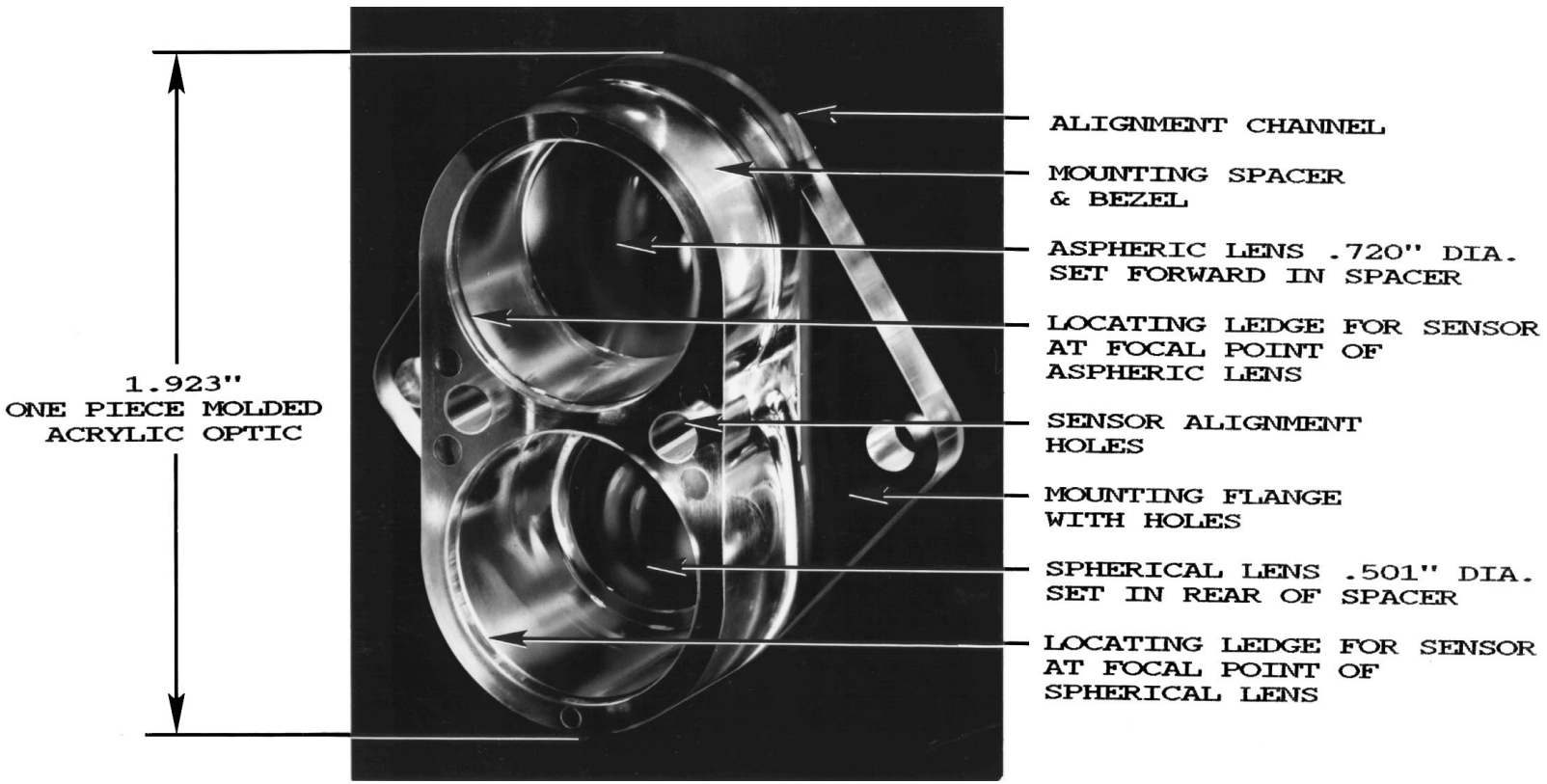

FIGURE 6.37 One-piece molded plastic assembly with two integral lenses, interfaces for sensors, and a mounting flange. (From 1983. *The Handbook of Plastic Optics*, 2nd ed. U.S. Precision Lens, Inc., Cincinnati, OH.)

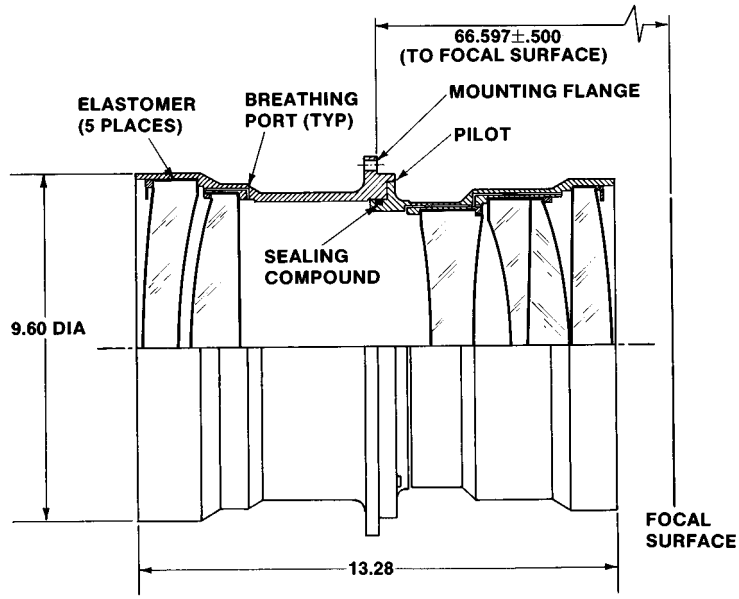

FIGURE 6.38 Partial sectional view of a photographic objective subassembly with elastomerically suspended lenses. (From Bayar, M. 1981. *Opt. Eng.*, 20, 181.)

Operational Motions of Lenses

In many optical instruments, internal adjustments are required during normal operation as, for example, to focus a camera or binocular on objects at different distances, to change focal length (and hence magnification) of a zoom lens, or to adjust focus of a microscope eyepiece to suit the observer's eye. Most of these adjustments involve axial motions of certain lenses or groups of lenses. A few applications, such as the range compensator of a camera rangefinder or rectification of converging images of parallel lines in architectural photography, may involve decentration and/or tilting of lenses.

Focus changes in a camera are generally achieved by moving the entire objective system relative to the film or by moving one or more lens elements within the objective relative to the rest of the lenses while the latter remain fixed with respect to the film. The required motions may be small or large depending upon the lens focal length and object distance, but these motions always must be made precisely and with minimum decentration of the moving elements.

Figure 6.39 shows schematically a typical mechanism used in a camera objective module to couple rotation of an external focus ring through a differential thread to move all the lens elements axially as a group. The differential thread comprises a coarse pitch thread and a slightly finer one on outer and inner surfaces of the intermediate cylinder. They act together to move the lenses as if they were driven by a fine pitch thread, but without the problems normally associated with manufacture, assembly, and possibly reduced lifetime of such a fine thread. The pitch of the equivalent fine thread equals the product of the actual pitches divided by the differences of those pitches.

Since they are used to observe objects at great distances, the optics of military telescopes, binoculars, and periscopes traditionally cannot be refocused for nearby objects. Calibration of reticle patterns used for weapon fire control purposes then remains constant. Whenever the magnification of such an instrument is greater than about 3 power, the eyepiece(s) is(are) individually focusable to suit the user's eye.

Many nonmilitary telescopes and binoculars utilize different means for focusing on objects at different distances. Since there is no reticle pattern to keep in focus, either the eyepiece or the objective can be moved for this purpose. The classical design for focusable binoculars, exemplified

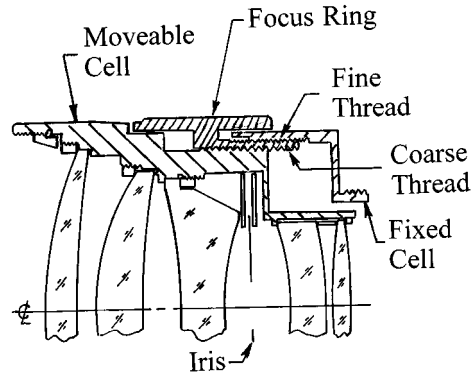

FIGURE 6.39 Simplified schematic sectional view of a camera objective featuring a differential thread focusing movement. Means for preventing rotation of the movable cell (a pin riding in an axial slot) is not shown.

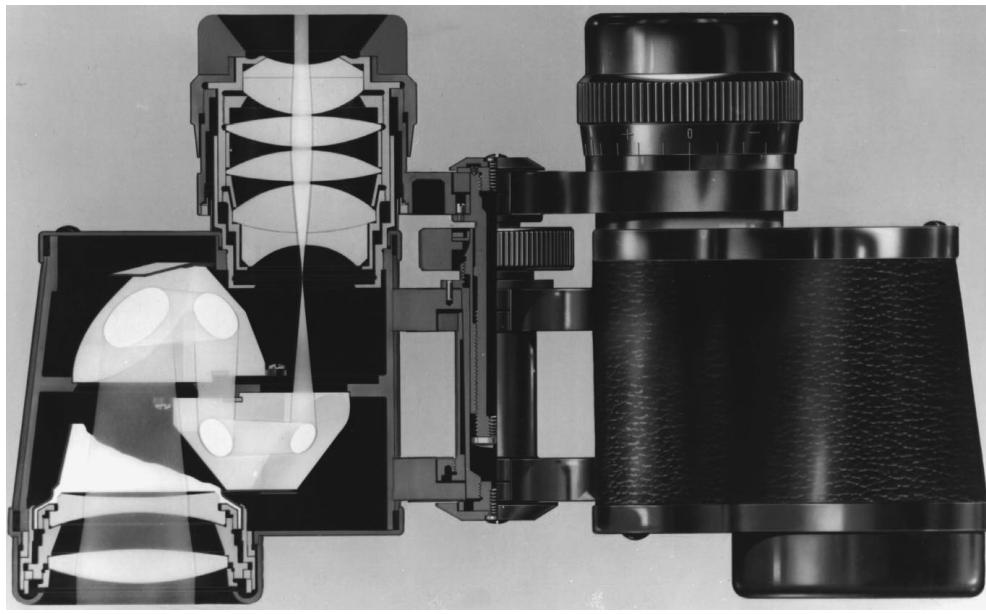

FIGURE 6.40 Partial section view of a commercial 8 × 30 binocular in which both eyepieces are moved axially to focus on objects at different distances. (Courtesy of Carl Zeiss, Inc., Aalen, Germany.)

by Figure 6.40, moves both eyepieces simultaneously along the axis as the knurled ring on the central hinge is rotated. One eyepiece has individual focus capability to allow accommodation errors between right and left eyes to be compensated in what is called the "diopter adjustment". The eyepieces in this design slide in and out of holes in the back cover plates on the prism housings. In low-cost binoculars, no attempt is made to seal the gaps between the eyepieces and these plates.

A more elegant approach for focusing a binocular is illustrated in Figure 6.41. Here, rotation of the focus ring on the central hinge moves internal lens elements of both objectives axially so as to adjust focus. Rotation of another knurled ring adjacent to the focus ring biases the position of the focusable lens of one objective so as to provide required diopter adjustment. Improved sealing is provided with this design since all external lenses can be sealed to the instrument housings.

Figure 6.42 shows an eyepiece for a low-cost commercial binocular in which the entire internal lens cell rotates on a coarse thread to move axially for diopter adjustment.[4] Figure 6.43 shows an eyepiece for a military binocular in which the entire internal lens cell slides axially without turning.

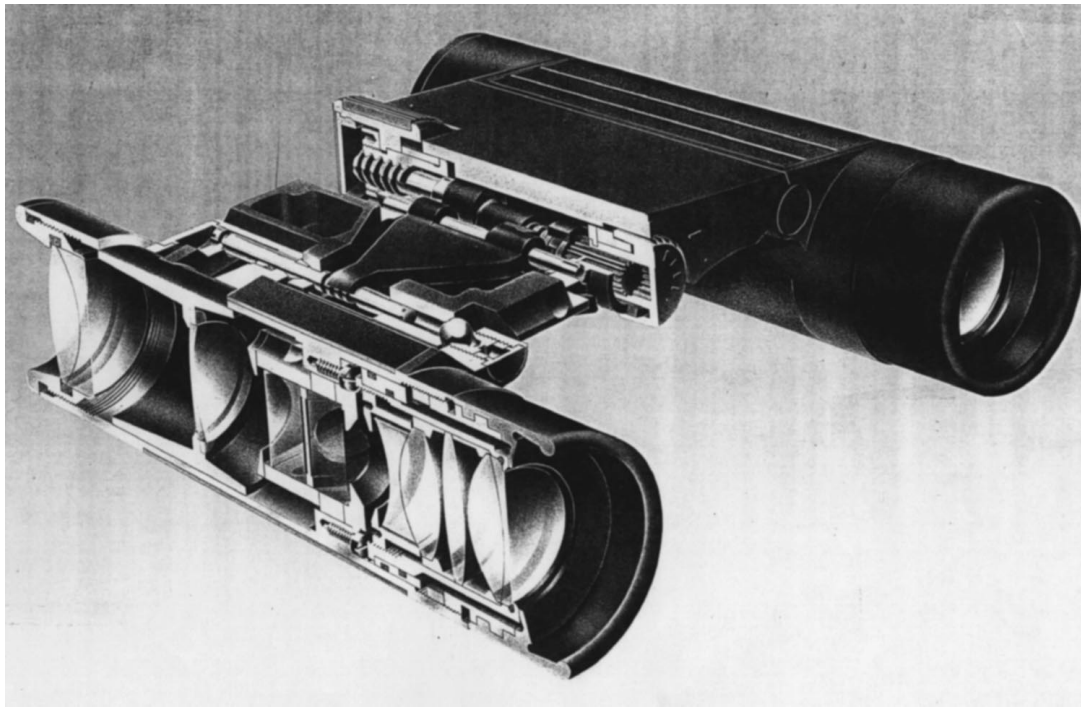

FIGURE 6.41 Partial section view of a commercial 8 × 20 binocular in which internal lens elements are moved axially to focus on objects at different distances. (Copyright: Swarovski Optik KG, Hall in Tirol, Austria. Used with permission.)

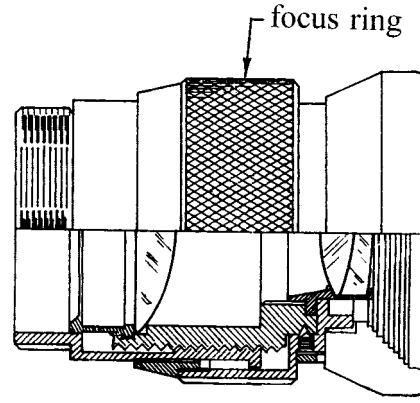

FIGURE 6.42 Simplified sectional view of an eyepiece for a commercial binocular in which the inner cell and lenses rotate on a coarse thread to focus. (Adapted from Horne, D.F., 1972. *Optical Production Technology*, Adam Hilger, Ltd., Bristol. *SPIE Proc. Vol. 163*, p. 92.)

The latter configuration has the performance advantage of maintaining better lens centration, but is more complex and so more expensive.

Most camera zoom lenses have two lens groups that move axially in accordance with specified mathematical relationships to vary the focal length and maintain image focus. Movement of a third lens group may adjust focus for different object distances. These motions usually are controlled by mechanical cams and driven manually by the operator. Smoothness of motion is very critical and lost motion (backlash) in the mechanism should be minimized.

Figure 6.44 shows a sectional view of a representative zoom mechanism. This lens was designed for use in the infrared and has four concentric cylinders machined as matched sets for straight

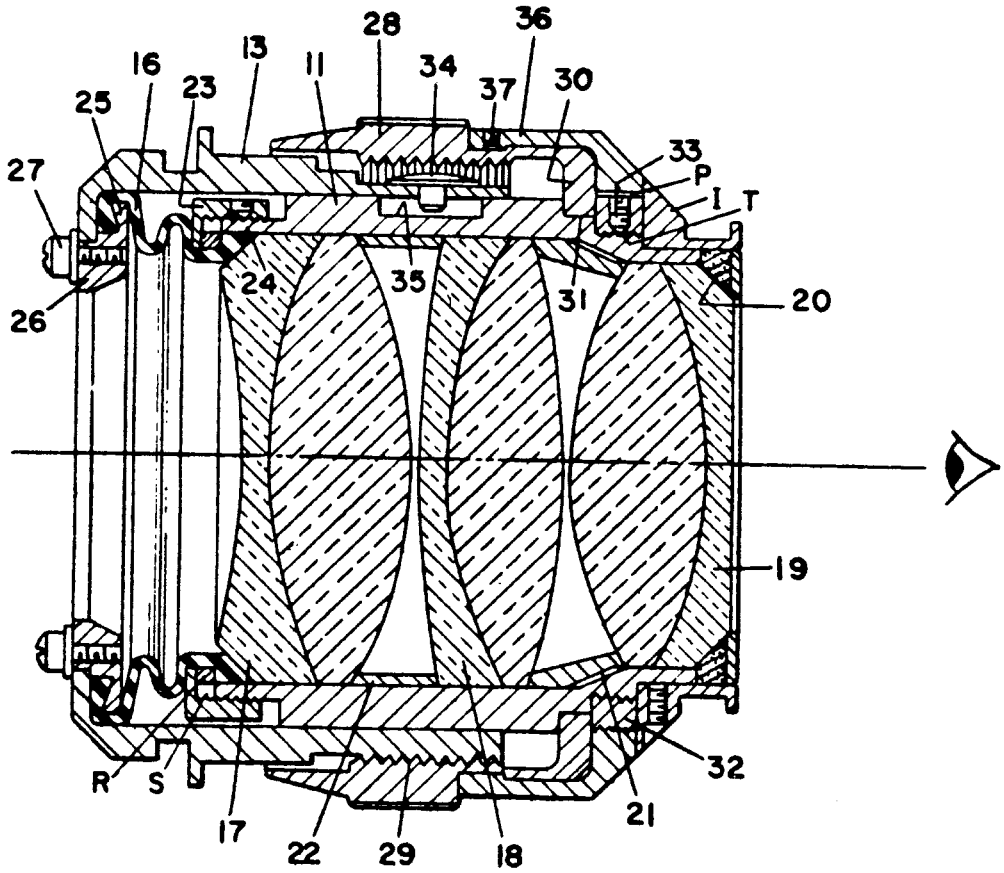

FIGURE 6.43 Simplified sectional view of an eyepiece for a military binocular in which the inner cell and the lenses are constrained by a pin (34) and slot (35) to move axially to focus without rotating. (From Quammen, M.L., Cassidy, P.J., Jordan, F.J., and Yoder, P.R., Jr. 1966. Telescope Eyepiece Assembly with Static and Dynamic Bellows-Type Seal, U.S. Patent No. 3, 246, 563.)

line motion of the movable lenses. It has independent cams to drive two lens groups. Close fits between the cam followers and cam slots are essential in all zoom lenses in order that the active lens motions agree adequately with their design relationships.[32,33] Particular care is taken to maintain contact between the followers and slots in cases where reversal of direction of motion occurs. Otherwise, perceptable image degradation and/or image displacement may occur at those points in the zoom motion.

Sealing Considerations

An important consideration in the design of optical instruments is keeping moisture, dust, and other contaminants from entering and depositing on optical surfaces, electronics, or delicate mechanisms. The need for protection from adverse environments depends upon the intended use. Military optical equipment is subject to very severe environmental exposures, whereas the optics used in scientific or clinical laboratories and in commercial and consumer applications (such as in interferometers, spectrographs, microscopes, cameras, surveyor's transits, binoculars, laser copiers and printers, compact disc players, etc.) usually experience a much more benign environment. The latter types of instruments generally have few, if any, provisions for sealing.

Static protection from the environment at normal temperatures can be provided by sealing exposed lenses and windows with cured-in-place elastomeric gaskets or O-rings. See Figures 6.8,

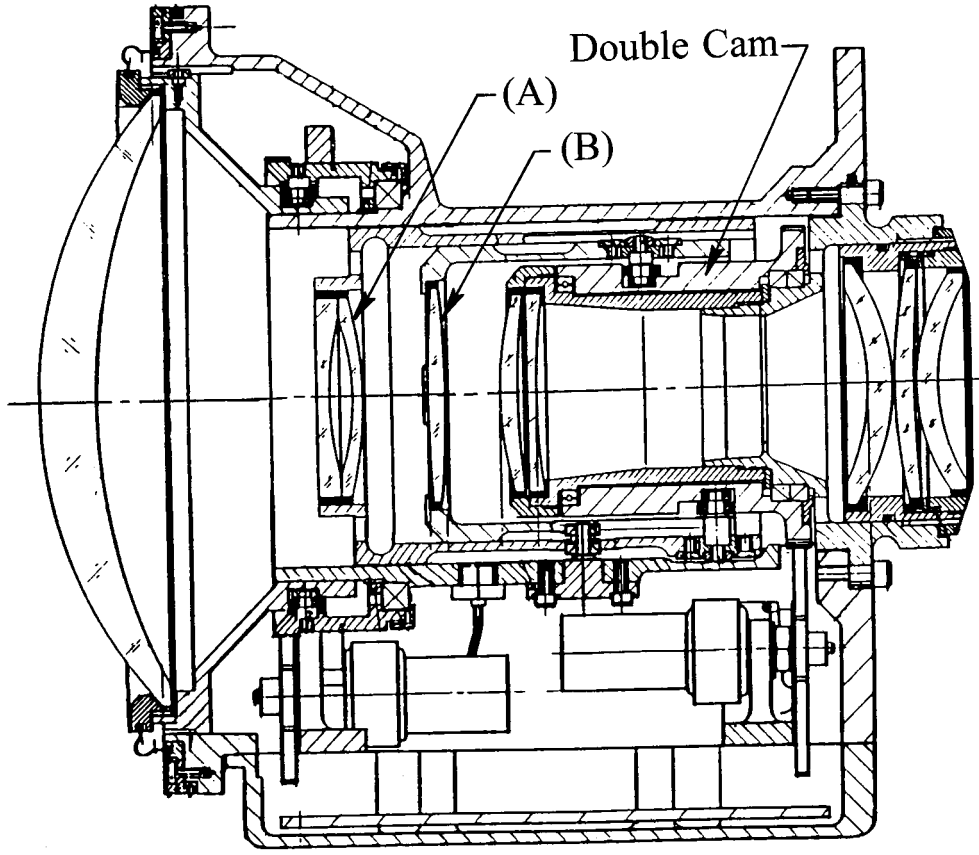

FIGURE 6.44 Simplified exploded view of a 10:1 zoom IR camera objective with two movable lens groups (A and B) each driven by a double-track cam to change focal length and maintain focus. (Adapted from Parr-Burman, P. and Gardam, A. 1985. *Infrared Technology and Applications, SPIE Proc. Vol. 590*, Baker, L.R. and Masson, A., eds., p. 11.)

6.30, and 6.36. Hermetic seals, such as may be required for hard-vacuum applications, are frequently created with gaskets made of indium, lead, or similar soft metals. An example of the latter is given in Section 6.4 ("Examples of Simple Window and Filter Mounts"). High temperature applications may require the use of seals made of formed resilient metal (such as gold-plated Inconel C-rings).[34] Nonporous materials are preferred for housings and lens barrels. Castings may need plating or impregnation with plastic resins to seal pores.

Exposed sliding and rotating parts are frequently sealed with dynamic seals such as O-rings, glands with formed lips, or a flexible bellows made of rubber or metal. In Figure 6.43, a rubber bellows seals the moving lens cell to the fixed housing at left while the outermost lens at right of the cell is sealed statically with an elastomeric seal. An O-ring inserted into the groove at the mounting flange seals the entire eyepiece to the instrument.[35]

Many sealed instruments are purged with dry gas such as nitrogen or helium as part of the assembly process. Positive pressure differential above ambient of perhaps 5 lb/in.^{2} (3.4×10^4 N/m^2) is sometimes generated within the instrument to help prevent intrusion of contaminants. Access through the instrument walls is, in this case, provided by a spring-loaded valve similar in function to those used on automobile tires.

Access for flushing of nonpressurized instruments can be by means of threading through holes into which seal screws are inserted after flushing. For example, two seal screws can be seen in each housing of the binocular shown in Figure 6.36.

Internal cavities of sealed instruments, such as those between lens elements, should be interconnected by leakage paths (bored holes, grooves, etc.) to the main cavity in order for the flushing process to work properly. Removal of moisture and/or products of outgassing from these ancillary cavities is facilitated if the instrument is evacuated and backfilled with the dry gas. Baking the instrument at elevated temperature for several hours also tends to eliminate these materials. To prevent potentially harmful pressure changes due to temperature changes, sealed instruments can be allowed to "breathe" through desiccators.[2]

Protection of outermost optical surfaces on cameras and electro-optical systems while not in use may be afforded by removable covers. Examples would include caps on personal binocular or camera lenses or ones placed over the apertures of airborne electro-optical sensors during takeoff and nonoperational phases of a military mission. The latter caps would be ejected before the instrument is put in use. Similarly, protective doors or covers are placed over exposed optics in space payloads prior to launch. These are opened mechanically or blown away upon reaching the orbit. In each case, the covers protect the optics from exposure to wind-driven dust, debris, and other abrasives as well as high velocity impact with rain, ice, and snow.

6.4 Mounts for Windows, Filters, Shells, and Domes

General Considerations

Generically, a window serves the very important function of isolating the interior of an optical instrument from physical damage and from adverse environmental conditions that may exist outside while allowing useful radiation to pass through. In its simplest form, the window is a plane parallel plate of optical glass, fused silica, crystals, or optical plastic. Shells and domes are special types of windows that have deep meniscus spherical or aspherical surfaces. Sometimes these components have zero net optical power even though the surfaces may be curved. In some applications, a window must mechanically support a positive or negative pressure differential between the outer and inner atmospheres. It may also constrain the internal environment as in the case of a gas laser tube, a spectrometer sample cell, or the observation port of a wind tunnel. An optical filter is another special type of window that serves to modify the spectral character of the transmitted radiation through selective absorption, reflection, or scatter.

The location of a window in the optical system determines to large extent the critical aspects of its design.[2,11] If located near an image plane, dirt, moisture, surface, and coating defects (scratches, digs, sleeks, or inadequate polish) may appear superimposed upon the image. The optical figure of the surfaces, wedge angle, and refractive index homogeneity of the material is less important in this case. If the window is located close to a pupil of the system, the relative importance of these characteristics is reversed, i.e., refractive properties are more important than cosmetic defects or surface contamination. Since, in most cases, windows and filters are relatively thin, their optical aberration contributions are relatively small, especially if located in collimated beams. If thick plane parallel windows are used in beams with large convergence or divergence they may contribute significant aberrations in the same manner as prisms.

Windows that are intentionally wedged to control spurious surface reflections or to deviate the beam in a specific direction may require special mounting arrangements to ensure proper orientation of the wedge apex. They may also cause spectral dispersion if the wedge angle is significant.

Environmental conditions surrounding a window affect its performance. For example, a window exposed to intense thermal radiation may develop a temperature gradient from side to side, front to back, or radially. These gradients tend to change the refractive properties and may change the physical shape of the element as well. Pressure differentials through the window also tend to change the shape of the element. For example, a window on an aerial camera exposed to rapidly moving air flowing over aircraft's skin may heat due to aerodynamic friction and bow into a meniscus shape. These effects might cause the camera image to go out of focus or otherwise deteriorate.

Table 6.3 lists important parameters to be considered in the design of optical windows. Only rarely would all these factors apply to a given case.

Table 6.3 Parameters of Importance in Optical Window and Filter Design

Transmission
Intensity loss throughout applicable spectral range
Blocking requirements for undesired radiation
Dimensions
Optical aperture (instantaneous and total)
Diameter or width and height
Thickness
Wedge angle and orientation
Special shape and/or bevel requirements
Optical properties
Optical power contribution
Transmitted wavefront quality requirements (or surface flatness/irregularity and index of refraction homogeneity)
Transmitted wavefront relative aperture (f/no)
Surface and bulk scatter characteristics
Coating requirements (reflectance, thermal emissivity, electrical)
Bubbles, inclusions, and striae
Polarization characteristics
Environment
Temperature extremes and exposure profiles (storage and operational)
Pressure (including ram air and turbulance effects)
Exposure to humidity, rain erosion, and particulate matter
Radiation (thermal, cosmic, nuclear)
Vibration (amplitude and frequency power spectral density)
Shock (amplitude, duration, and direction)
Mounting configuration
Orientation relative to optical beam(s) and vehicle motion
Mechanical stresses induced (operation and storage)
Thermal properties of materials
Heat transfer mechanisms and paths
Mechanical interface (mounting hole pattern)
Sealing requirements

Adapted from Yoder, P.R., Jr. 1985. *Geometrical Optics, SPIE Proc. Vol. 531*, Fischer, R.E., Price, W., and Smith, W.J., eds., p. 206.

Rather than to review these items individually, a few representative window configurations are described from the optomechanical viewpoint. The interrelationships between different applications and technical requirements are stressed. Although important, windows and filters for use in high energy laser systems are intentionally omitted from consideration because space limitations preclude adequate treatment of those topics. The windows fused in place for applications such as gas discharge laser tubes are also omitted.

Examples of Simple Window and Filter Mounts

A large variety of plane-parallel plates made of glass, crystals, etc. are available as catalog items from optical component manufacturers to meet many needs for windows to be used in optical instruments, laboratory experiments, and for other purposes. They can be purchased in standard sizes and uncoated or antireflection coated. Needs for components not available directly from a catalog can frequently be met by modification of standard parts to special order. If this approach is unsuccessful, the needed parts can be custom fabricated to print.

Figure 6.45 shows a plane-parallel window intended to cover the aperture of a visual telescope, to protect the significantly more expensive nearby objective lens from damage, and to prevent

entrance of moisture and other contaminants from the military environment.[36] Its diameter is nominally 52 mm (2.05 in.), its aperture is 48 mm (1.89 in.), and its thickness 8.8 mm (0.346 in.). It is mounted in a stainless steel cell designed for flange mounting to the telescope housing. The window is clamped in the cell by a threaded stainless steel retainer and subsequently sealed with injected elastomer per the referenced military specification. The cell, in turn, is bolted to the telescope housing and sealed with an O-ring that fits into the groove shown on the flange. The subassembly is intended to maintain a positive pressure within the telescope of at least 5 lb/in.^{2} (3.45×10^4 N/m$^{2)}$ over external ambient pressure.

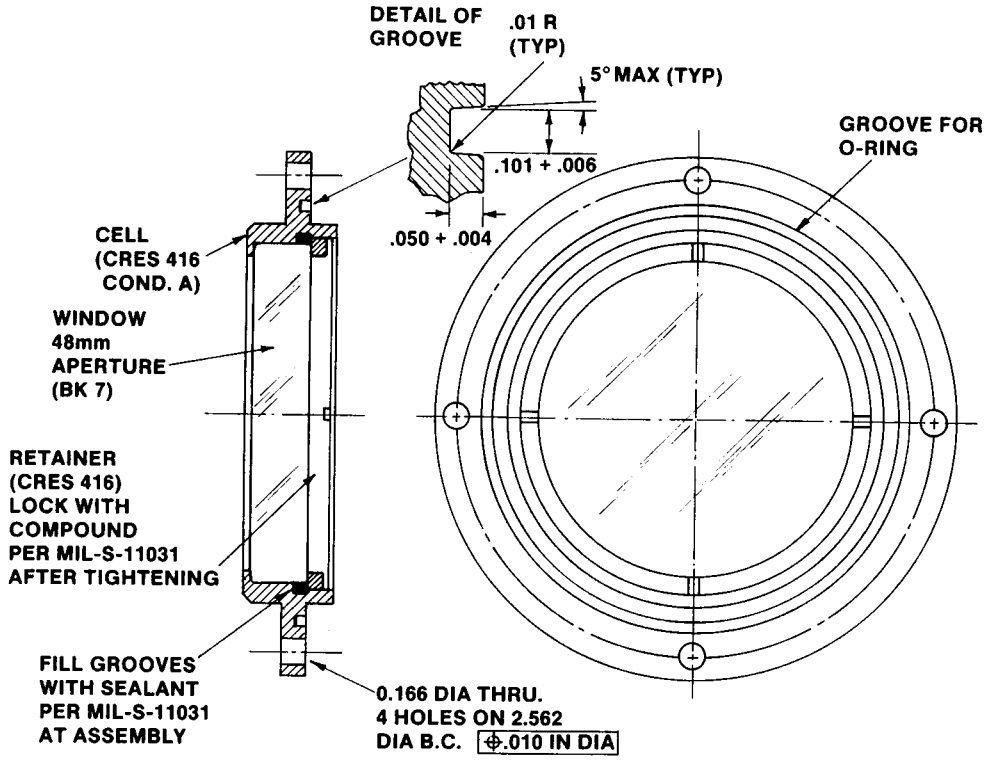

FIGURE 6.45 Instrument window subassembly with window held in place by a retaining ring and sealed with an elastomer. (From Yoder, P.R., Jr. 1985. *Geometrical Optics, SPIE Proc. Vol. 531*, Fischer, R.E., Price, W., and Smith, W.J., eds., p. 206.)

Because the window is located in a collimated beam near the telescope's pupil (which is at the objective) and its aperture is always filled, the maximum transmitted wavefront error is specified as ±5 waves optical power and 0.05 wave peak-to-valley irregularity in 633-nm laser light. Maximum wedge angle is specified as 30 arc seconds. By choosing high quality optical glass for the window (in this case BK7 borosilicate crown) the designer is ensured a high degree of refractive index homogeneity, freedom from striae, bubbles, and inclusions, adequate climatic resistance of the substrate, ease of fabrication, and reasonable material cost. Antireflection coatings of magnesium fluoride provide high durability.

One solution to the problem of providing a vacuum-tight, chemically inert mounting for an infrared crystal window in a stainless steel instrument housing for multiple-photon laser-induced chemistry in gaseous media[37] is illustrated in Figure 6.46. The window is a 7.6-cm (3-in.)-diameter disk of single crystal or polycrystalline sodium chloride approximately 9 mm (0.35 in.) thick. During long-term use, this window was intended to hold internal vacuum of a few millitorr pressure at temperatures of 200 to 275°C with helium leak rates of the order of 3×10^{-10} atm-cm^3/sec while

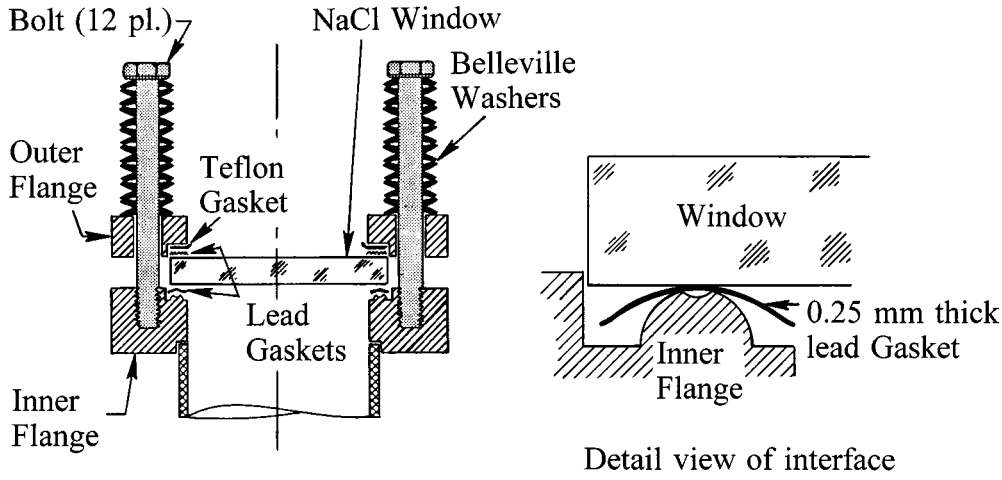

FIGURE 6.46 Diagrams of a high-temperature, vacuum-sealed infrared window subassembly. (Adapted from Manuccia, T.J., Peele, J.R., and Geosling, C.E. 1981. *Rev. Sci. Instrum.*, 52, 1857.)

the sample was being irradiated with pulsed laser radiation. Resistance to thermal shock from 1°C/min temperature changes also were required.

The window surfaces were clamped between two thick stainless steel flanges by 12 Belleville spring-loaded bolts to provide uniform axial pressure and flexibility to accommodate thermal expansion mismatch between the materials. The window was not constrained transversely other than by friction. The inner window surface was sealed to the inner flange through a 0.25-mm (0.010-in.)-thick gasket of lead. The flange had the unique shape described in the detail view. A convex annular toroidal interface 1.9 mm wide projecting from the flange surface was provided with a concave annular groove of 0.19-mm (0.008-in.)-depth. Under compression at high temperature, the edges of the groove cut through the gasket and trap a ring of lead under high hydrostatic pressure inside the groove, where it extrudes into microscale irregularities of the window and of the flange surfaces forming a vacuum seal. The interface between the outer surface of the window and the flange had a 0.25-mm (0.010-in.)-thick lead gasket and a 0.125-mm (0.005-in.)-thick Teflon™ gasket. The surfaces of that lead gasket were roughened so it would deform under preload to distribute the axial force over a large area of the window.

Figure 6.47 shows a much simpler mounting configuration; this for a set of four glass spectral filters each with 25.4 mm (1.00 in.) clear aperture and 3 mm (0.12 in.) thickness located in a multiple-aperture filter wheel inside a laboratory optical system. Since there is no need to seal the filter or even to precisely control its location and/or orientation relative to the optical axis for the intended application, each optical element is held in place by a spring-type snap ring (see Section 6.2 [“Low Precision Mounts” — “Snap Ring”] and Figure 6.3). The wheel is driven manually from one location to another with positioning at 90° intervals determined by a spring-loaded ball (not shown) dropping into the “V” detents shown on the wheel rim. The laboratory environment to which the instrument is exposed is relatively benign and the glass-to-metal interfaces are loose so there are no significant mounting stresses. If it were expected that the filters would not need to be removed during the lifetime of the assembly, they might well be sealed in place with an elastomer.

Example of A Larger Window Mount

Cameras and electro-optical sensors used in high-performance military aircraft are usually mounted on stabilized mounts within environmentally controlled equipment bays in the fuselage or in externally mounted pods. Windows are needed to seal the bay or pod and to provide

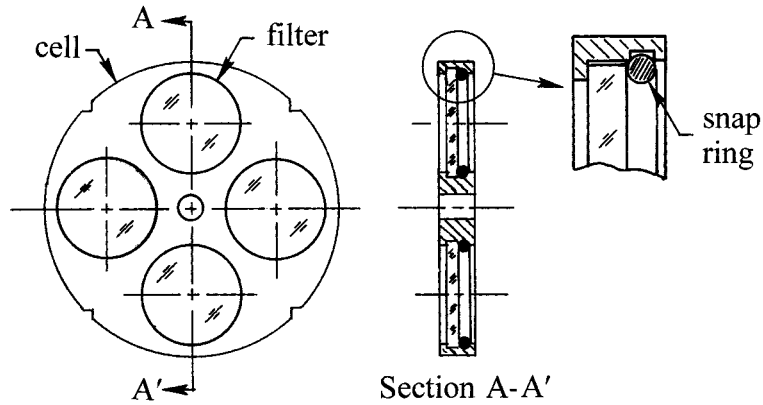

FIGURE 6.47 Schematics of a simple multiple-filter wheel subassembly.

aerodynamic continuity of the enclosure. In this section, an example of such a special design is considered.

The multi-aperture window assembly shown in Figure 6.48 is designed for use in a military aircraft.[36] The larger window is used by a forward-looking infrared (FLIR) sensor and is made of antireflection-coated chemical-vapor-deposited (CVD) zinc sulfide (ZnS). It measures approximately 30 × 43 cm (11.8 × 16.9 in.) and is 1.6 cm (0.63 in.) thick. The irregular aperture conforms with the footprint of the 25.4-cm (10-in.)-diameter beam entering the sensor's optical aperture at the nominal angle of incidence of 47°. The smaller windows are used by a laser range finder/target designator system operating a 1.06-μm wavelength. These windows are identical, have apertures of 9 × 17 cm (3.5 × 6.7 in.), have thicknesses of 1.6 cm (0.63 in.), and are fabricated of BK7 glass. They also are antireflection coated. Specifications for transmitted wavefront error (including mechanical deformations caused by mounting) are 0.1 wave peak-to-valley at 10.6 μm over the beam diameter for the ZnS window and 0.2 wave peak-to-valley power plus 0.1 wave irregularity at 632.8 nm over the full aperture for the BK7 windows.

For maximum strength under environmental and operational stress, all window surfaces (including the rims) are carefully fabricated by the "controlled grinding" process[38,39] in which progressively finer abrasives are used to remove all traces of subsurface damage caused by the preceding grinding operation. Each window is elastomerically bonded into close-fitting recesses in a contoured anodized 6061-T651 aluminum plate. This plate is bolted to a matching machined interface on the aircraft structure to minimize bending that could stress the refracting materials and distort their optical surfaces.

Examples of Shell and Dome Mounts

Meniscus-shaped optical elements are frequently used as windows for electro-optical sensors having wide fields of view or those with smaller instantaneous fields that are scanned over wider conical fields. Generically they are shells; very deep shells are called domes. Domes subtending >180° from their centers are called hyperhemispheres. Because of their shapes, shells are stiffer than flat windows of the same thickness.

Many shells and domes are made of optical glass and function at visible wavelengths. Others are used in the infrared so must be made of crystalline materials such as zinc selenide, zinc sulfide, germanium, or silicon. Some infrared-transmitting materials are soft and so are difficult to polish and not very resistant to erosion due to impact with dust, rain, ice, or snow at high velocities.[40] Composite substrates such as soft zinc selenide coated with a layer of harder zinc sulfide are sometimes used to combat the latter problem. Shallow shells are frequently used as aberration correctors in objective systems such as Maksutov telescopes.

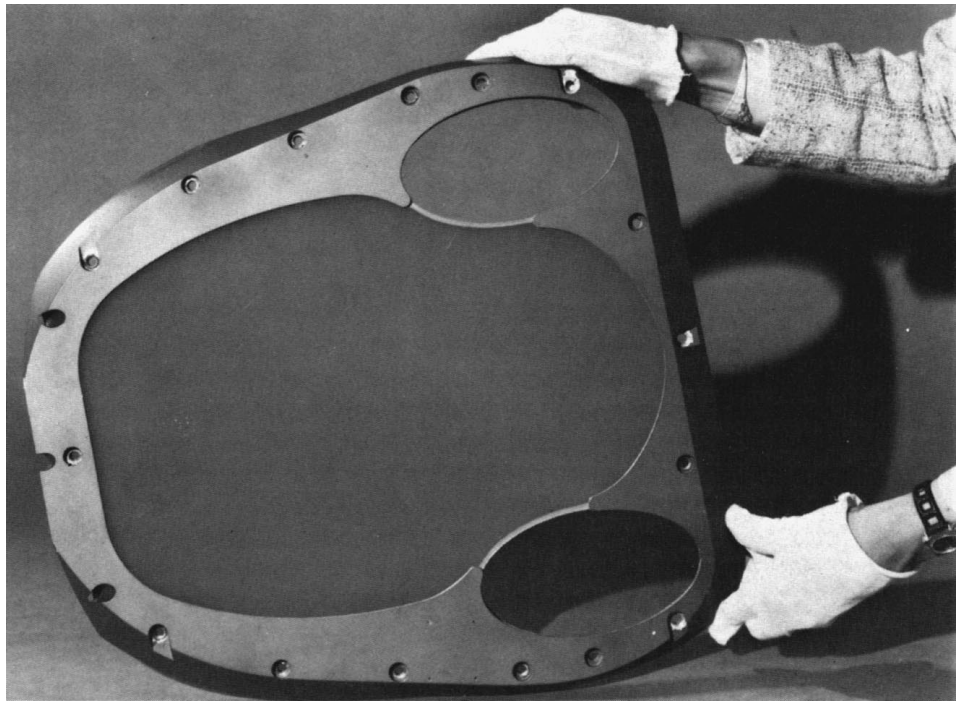

FIGURE 6.48 A multi-aperture window subassembly for a military multiwavelength electro-optical sensor. (From Yoder, P.R., Jr. 1985. *Geometrical Optics, SPIE Proc. Vol. 531*, Fischer, R.E., Price, W., and Smith, W.J., eds., p. 206.)

Mountings for shallow and deep shells typically involve elastomeric potting techniques or mechanical clamping with flange-type retaining rings.[2,11,36] Three examples are shown in Figure 6.49. View (A) shows a crown glass hyperhemisphere with its shaped rim potted into a flange that is, in turn, attached to structure with several bolts. An O-ring seals the flange to the structure. The pilot diameter indicated in the figure serves to center the optical element to the axis of the system. View (B) shows a shallow dome clamped with a Delrin ring to a housing with a series of Nylon screws. A molded Neoprene gasket seals the optic to the mount. View (C) shows a zinc sulfide dome bonded with epoxy to a bezel and supported axially by a threaded retaining ring. This design was successfully used on a projectile fired from a mortar with approximately 11,000-G accelerations.[41]

Pressure Differential Effects

Pressure differentials through flat and curved windows tend to change the shapes of the optical surfaces; these can adversely affect the performance of the optical systems using the windows by distorting the transmitted wavefront. These shape changes also introduce tensile and compressive stresses into the refracting materials. As discussed in Section 6.2 ("Axial Stress at Single Element Interfaces" — "Bending Stress Due to Preload"), tensile stresses are more serious than compressive stresses and may lead to failure.

Vukobratovich[11] outlined techniques for estimating (1) the optical path difference introduced into a wavefront passing through a flat window when that window is deformed by a given pressure differential and (2) the stress introduced into the window by that deformation. He indicated that, for a given window diameter/thickness aspect ratio, in visible light systems, pressure-induced wavefront distortion may outweigh pressure-induced stress effects, while in infrared systems, the reverse may be true because of the less stringent requirements for optical surface figure in the latter

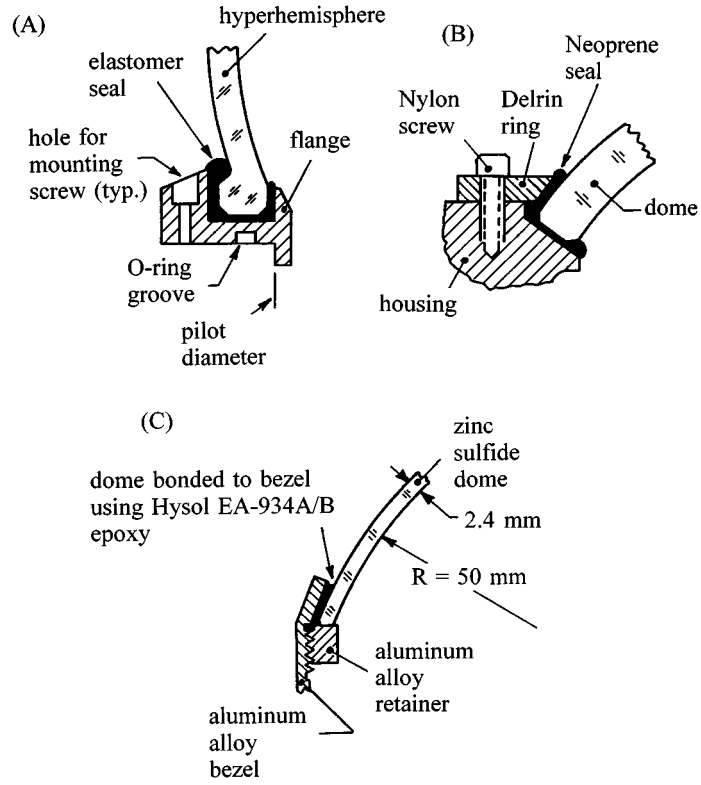

FIGURE 6.49 Three configurations for dome mounting interfaces. (A) Hyperhemisphere potted into a flange. (From Yoder, P.R., Jr. 1993. *Opto-Mechanical Systems Design*, 2nd ed. Marcel Dekker, New York.) (B) Dome clamped by an external ring. (From Vakobratovich, D. 1986. *Introduction to Optomechanical Design, SPIE Short Course Notes.*) (C) Dome bonded in place and clamped by an internal retainer. (From Speare, J. and Belloli, A. 1983. *Structural Mechanics of Optical Systems, SPIE Proc. Vol. 450*, Cohen, L.M., ed., p. 182.)

systems. He also provided a good summary of means for estimating the probability of window failure under a given stress.

A typical application involving large pressure differentials is a window for a deep submergence vehicle. Usually these windows are made of polymethyl methacrolate (acrylic), are quite thick, and have limited aperture. Their rims usually are tapered and closely matched in angle and surface roughness to the interfacing mechanical surface. This allows the window to move axially and avoids hoop stress effects from thermal expansion mismatch under temperature changes. Figure 6.50 shows an example of a window with a 90° taper.[42] The Neoprene gasket seals the window in place at normal pressures; at large underwater depths, the window is driven solidly against and sealed into the mount. Under extreme pressure differentials, the window tends to extrude through the inner mount aperture of diameter D. It is not uncommon for window thickness, d, to be 50% of D.[43]

Domes subjected to large pressure differentials develop stress and may collapse due to elastic buckling.[11]

Thermal Effects

Temperature stabilization of high performance optical systems is important to prevent deterioration of image quality. The segmented window shown in partial section view in Figure 6.51 is an example of design for this purpose.[2] It is used on a high speed military aircraft as part of a high resolution panoramic photographic reconnaissance system capable of scanning from horizon to horizon through nadir transverse to the flight direction. In this example, dual 1-cm (0.39-in.)-

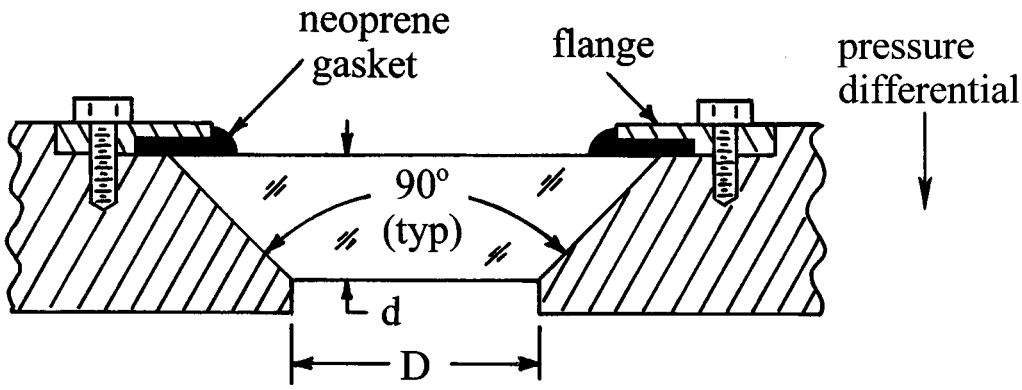

FIGURE 6.50 A tapered-rim acrylic window subassembly intended for a deep-submergence application involving a large hydrostatic pressure differential. (From Vukobratovich, D. 1986. *Introduction to Optomechanical Design, SPIE Short Course Notes.*)

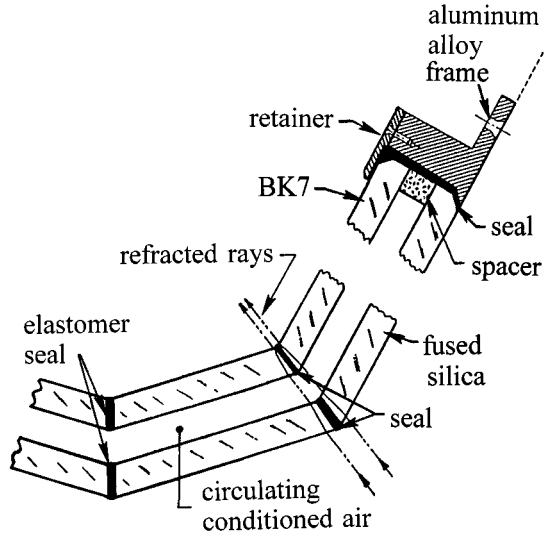

FIGURE 6.51 Partial schematic of a double-glazed, multisegment window subassembly intended for a horizon-to-horizon panoramic aerial camera application. (Adapted from Yoder, P.R., Jr. 1993. *Opto-Mechanical Systems Design*, 2nd ed. Marcel Dekker, New York.)

thick glazings in "thermopane" configuration serve to stabilize the temperature of the camera's environment. The outer glazings are made of fused silica. They carry a low-emissivity (gold) coating on their interior surfaces to minimize transfer of heat to the camera from the windows' outer surfaces as the latter are heated by boundary layer friction during high speed flight. The inner glazings are made of BK7 glass. They are coated for maximum transmission in the spectral region surrounding the peak sensitivity of the film. Further thermal stabilization is afforded to the window, and hence to the camera optics, by passing conditioned air from the aircraft's environmental control system through the air space between the glazings.

The square glazings at the center of each window measure approximately 32 × 33 cm (12.6 × 13.0 in.), while the side glazings are slightly smaller. All window surfaces are processed by the "controlled grinding" method to maximize strength.[38,39] These glazings are sealed with elastomer into recesses machined into an aluminum frame. The frame is contoured to fit closely to a matching machined interface on the aircraft's camera pod and is secured with several bolts.

Under natural (such as solar irradiation) or artificial heating (as in an attempt to stabilize temperature), the window itself may become distorted by axial or transverse thermal gradients, thereby causing the transmitted wavefront to be defocused and deformed. Barnes explained how to estimate the optical path differences introduced by these gradients in circular aperture windows used in high-acuity spaceborne systems.[44] He indicated that, in general, windows should be as thin as possible and the physical aperture should be significantly larger than the optical aperture. The equations given by Barnes were summarized in a more recent publication by Vukobratovich.[11] Rectangular aperture windows with temperature gradients will, in general, deform the transmitted wavefront asymmetrically and introduce astigmatic focus errors.

An example of a mounting arrangement that has a designed-in radial thermal gradient is shown in Figure 6.52. Here, a circular aperture segmented optical interference filter is heated a few degrees above the highest specified ambient by a thermostatically controlled heater coil mounted within the cell wall. The cell is fabricated from a phenolic insulating material (G10) and mounted to an aluminum structure.[2]

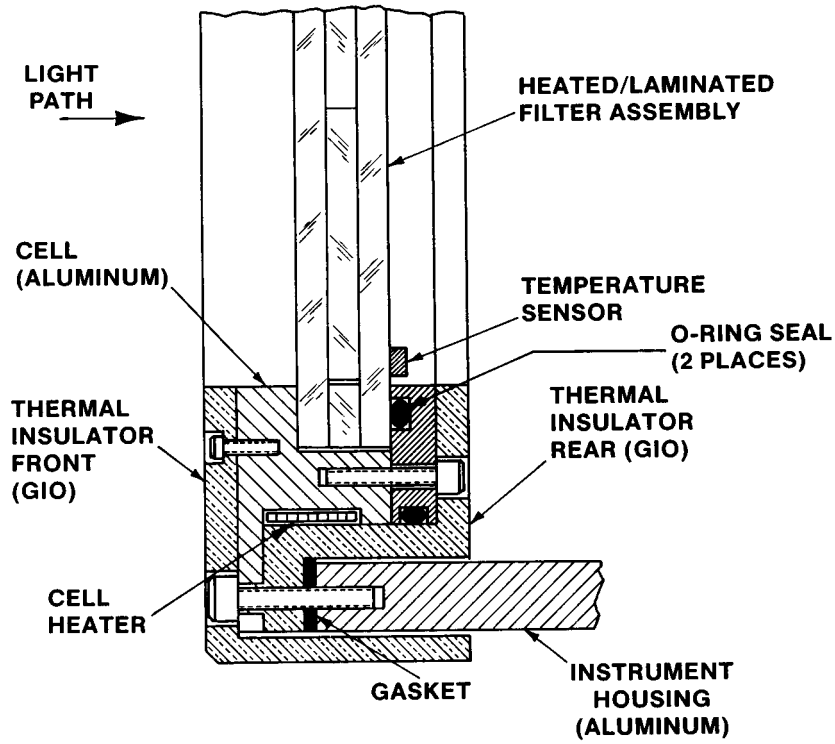

FIGURE 6.52 Schematic of a window (interference filter) mount with active temperature stabilization means. (From Yoder, P.R., Jr. 1993. *Opto-Mechanical Systems Design*, 2nd ed. Marcel Dekker, New York.)

6.5 Mounts for Small Mirrors

Clamped Mounts

A kinematic support for a body has six independent constraints, one each for the six degrees of freedom in inertial space (three rotations about mutually perpendicular axes and three translations along those axes). Ideally, contact with the body occurs at points so moments cannot be exerted thereon. When restraining forces are delivered over very small areas (points), the loads per unit area become large, stresses develop, and elastic bodies can be deformed. To prevent this from

becoming a problem in mounting optical elements, finite-sized contact areas are used. The mount is then called semikinematic.

To illustrate a semikinematic mount for a small flat mirror, consider the concept shown schematically in Figure 6.53. Here a circular mirror is clamped between three spring-loaded pads and three coplanar fixed pads located directly opposite through the mirror. The pads are located at 120° intervals on the mirror's surfaces. The contact areas on both sides of the mirror are small and the force vectors pass centrally through those contact areas and perpendicular to the mirror surfaces. These forces constrain the mirror against one translation and two rotations. Two spring-loaded pads press perpendicularly against the rim of the mirror to hold it against a single opposing rigid pad. The rim-contacting pads, shown oversize, lie in the plane of the mirror's center of gravity at 120° intervals. They constrain the mirror against the other two translations. Note that the locations of all pads are adjustable and the adjustments have locking setscrews. This allows the mirror to be centered radially and the spring forces to be adjusted at assembly.

Since this is a flat, symmetrical mirror, rotation about the third axis (normal to the mirror) is not critical. Nevertheless, that motion also is constrained somewhat by friction at the contact areas. In some flat mirror designs, all rim contacts are omitted and friction depended upon to hold the mirror against two translations as well as the one rotation. Direct radial constraint would be appropriate for spherical or aspherical mirrors since centration is important in those cases.

If possible, the reflecting surface of a first-surface mirror should contact the fixed pads rather than the spring-loaded ones. Then wedge in the mirror substrate will not affect alignment of the reflected beam if the mirror rotates about an axis perpendicular to its face. In the case of a second-surface mirror, registering the reflecting surface is again advisable, but some light beam deviation is introduced by substrate wedge.

Frequently the springs that hold the mirror are flat blades (clips) of beryllium copper or spring steel. The force, F, delivered to the mirror by each clip is then determined by treating it as a deflected short cantilevered beam.[2,9] The following equation gives the deflection, x, required to produce a given force:

$$x = \left(1 - \upsilon^2\right)\left(4FL^3 / Ebh^3\right) \tag{35}$$

where

- υ = Poisson's ratio for the spring material
- F = applied force per spring
- L = free length of beam
- E = Young's modulus for the spring material
- b = width of spring
- h = thickness of spring

In this equation, h is assumed to be small compared to b.

Bonded Mounts

Techniques for mounting small mirrors by glass-to-metal bonding with adhesive such as epoxy have gained considerable popularity, especially for military and aerospace applications involving exposure to severe environmental conditions. They are frequently used for nonmilitary applications because of their ease of assembly and durability.

The simplest form of bonded interface is at the back surface of a first-surface mirror. Such a design is shown in Figure 6.54. Here, the fine ground back surface of a 2-in. (5.1-cm)-diameter, 0.33-in. (0.84-cm)-thick crown glass mirror is bonded to an elevated flat circular pad on a stainless steel bracket with epoxy adhesive approximately 0.004 in. (0.10 mm) thick. The area, Q, of the pad is 0.5 in.^{2} (3.2 cm^2). The weight, W, of the mirror is approximately 0.09 lb (0.041 kg).

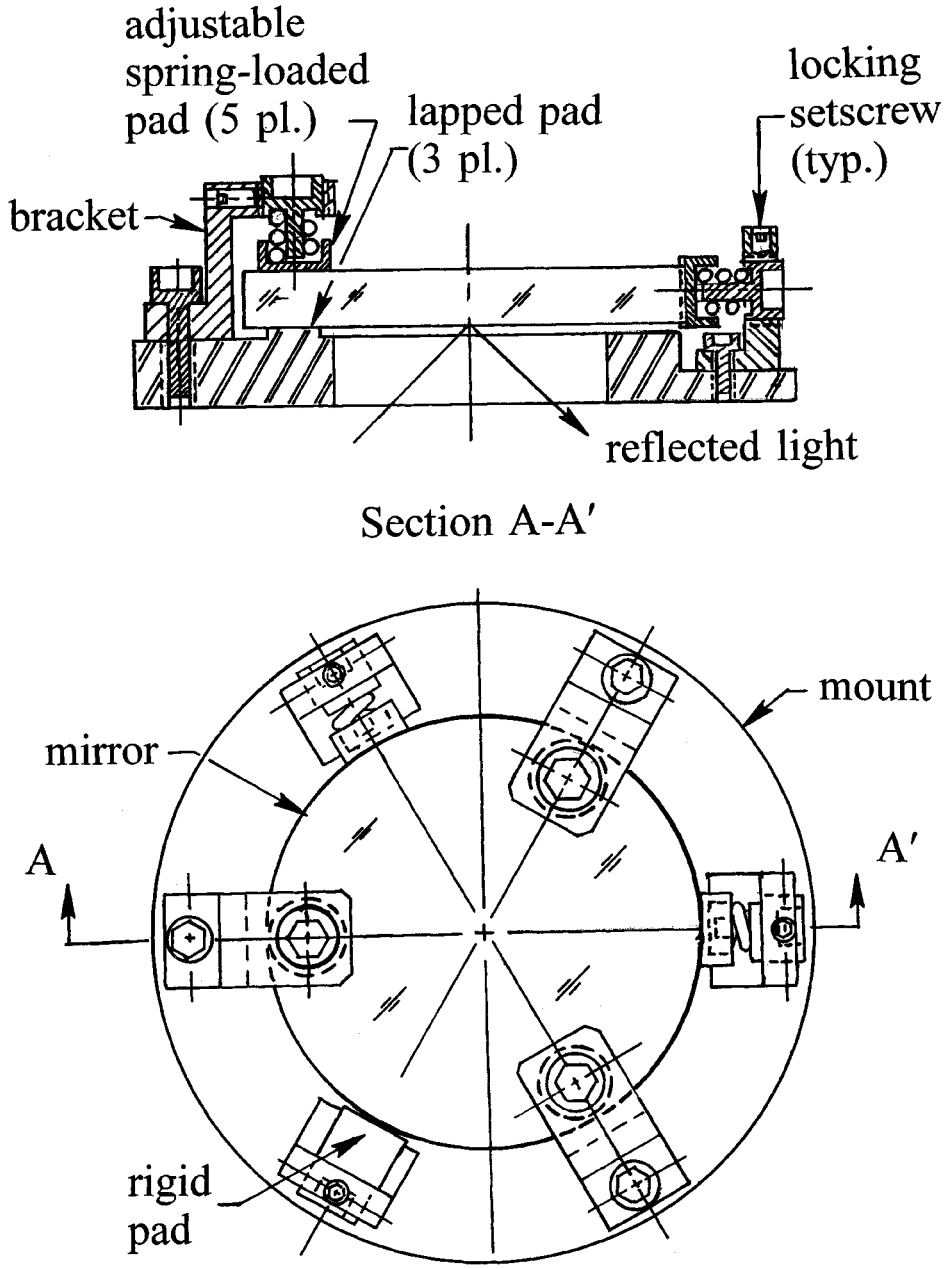

FIGURE 6.53 Schematic of a spring-loaded mounting for small, circular, flat mirrors.

The adequacy of a bond such as this can be established as follows. Under directional acceleration of "G" times gravity, the mirror exerts a tensile or shear stress upon the bond of GWS_F/Q in units of lb/in.^{2} (or N/m^2), where S_F is a safety factor. This stress can be compared to the strength of the adhesive joint, J, which, for many epoxies, is of the order of 2000 lb/in.^{2} (1.38×10^7 N/m^2). The magnitude of Q for a given S_F is given by:

$$Q = GWS_F / J \tag{36}$$

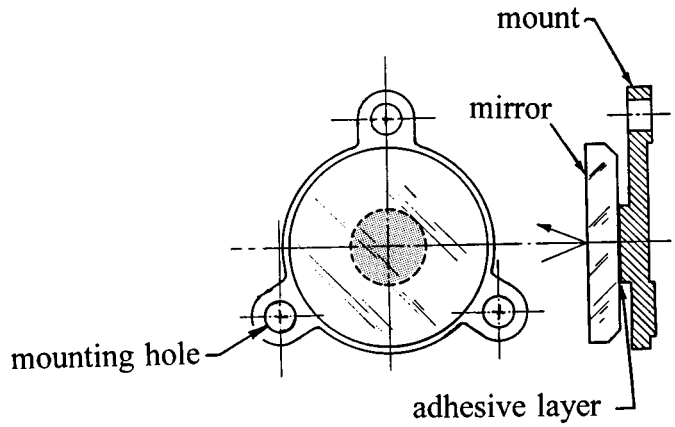

FIGURE 6.54 Typical construction of a first-surface mirror subassembly with glass-to-metal adhesive bond (shaded area) securing the back of the mirror to the mount. (From Yoder, P.R., Jr. 1985. *Geometrical Optics, SPIE Proc. Vol. 531*, Fischer, R.E., Price, W., and Smith, W.J., eds., p. 206.)

Experience indicates that S_F should not be less than 2 and perhaps should be as large as 10 to compensate for hard-to-control assembly conditions such as inadequate cleanliness of the interfacing surfaces.[2] In the example above, an acceleration as large as 1110 times gravity will allow S_F to equal 10.

Since all adhesives tend to shrink somewhat during cure and the shrinkage in a given direction is a small percentage of the corresponding maximum dimension of the bond area, it is desirable to keep the bond area as small as practical. This also may tend to speed the curing process with some adhesives. One accepted technique for minimizing bond area is to determine the total bond area required and then to divide this into three equal subareas arranged in a reasonably large triangular array on the mirror surface. This distribution is somewhat kinematic and helps to stabilize the assembly.

Since the coefficient of thermal expansion of the adhesive is significantly larger than those of the mirror or the mount, it can contract significantly as the temperature drops. It is best if excess adhesive is not allowed to extend beyond the bonding pad on the mount so as to form a fillet of adhesive "bridging" to the mirror. Experience has shown such fillets to be the cause of glass fracture at low temperatures. Careful application of a predetermined adhesive volume and/or prompt removal of excess uncured adhesive minimizes this potential problem.

Achievement of a uniform adhesive layer thickness is facilitated by such means as building localized pads or hard registration points of the proper height into the mount, by installing temporary shims between the mirror and mount or by mixing spherical beads of glass or similar material having the proper (small) diameters into the adhesive prior to application. In order to minimize shrinkage effects perpendicular to the bond area during cure, the thickness of the bond is frequently held to a small value such as 0.004 in. (0.10 mm) to 0.015 in. (0.38 mm). Exceptions to this "rule" include choice of bond thickness to athermalize the assembly (as discussed in Section 6.2 ["Elastomeric Suspension Interfaces" for lenses) or to provide a limited degree of shock resistance by virtue of the resiliency of the adhesive.

Flexure Mounts

To allow for thermal expansion coefficient variations between mirrors and mounts, flexures are frequently designed into the mounts. Figures 6.55 and 6.56 illustrate two such mounting arrangements.

In Figure 6.55, three rectangular metal pads are bonded to the edge of a rectangular aperture mirror. Three flat flexure blades attach the pads to the instrument structure (baseplate). The blades

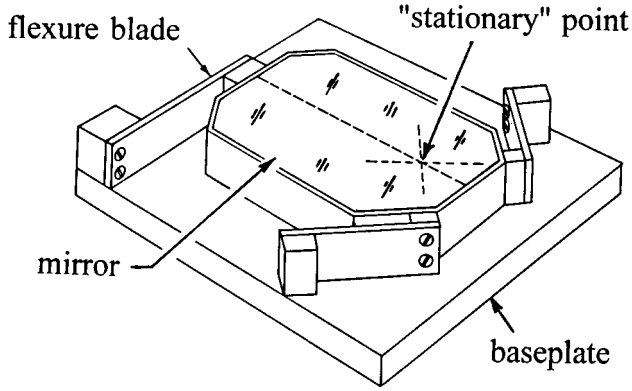

FIGURE 6.55 Concept for a flexure-mounted rectangular mirror subassembly. (From Yoder, P.R., Jr. 1985. *Geometrical Optics, SPIE Proc. Vol. 531*, Fischer, R.E., Price, W., and Smith, W.J., eds., p. 206.)

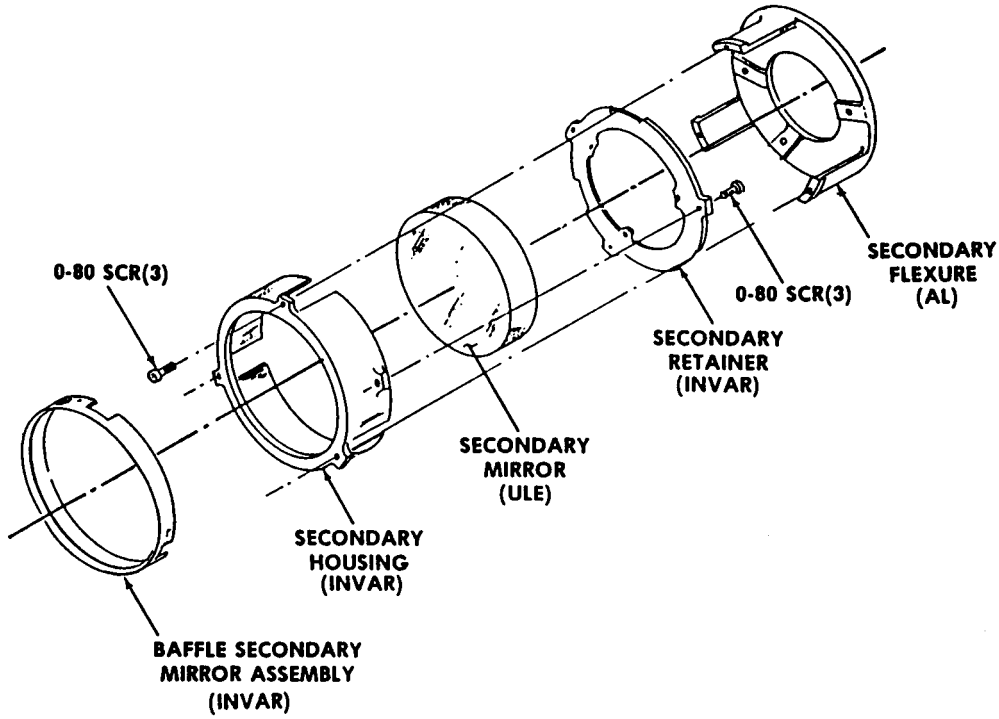

FIGURE 6.56 Exploded view of a flexure-mounted telescope secondary mirror intended for a space application. (From Hookman, R. 1989. *Precision Engineering and Optomechanics, SPIE Proc. Vol. 1167*, Vukobratovich, D., ed., p. 368.)

are stiff in the directions of their lengths and depths, but relatively flexible in the directions of their thicknesses. If the baseplate and mirror combination have different coefficients of thermal expansion, temperature changes will cause the flexures to bend, but minimal forces will be exerted upon the mirror. The bending motions are typically along arcs of radii equal to the free lengths of the flexures. If these arcs meet at a point (as shown schematically in the figure), that point will tend to remain stationary with temperature change. Ideally, this point should coincide with the center of gravity of the mirror.[2]

In Figure 6.56, a circular aperture ULE® mirror is clamped with a retainer into an Invar cell which is then attached to the ends of thin flexures machined into a circular aluminum mount.

Since the materials differ greatly with regard to CTEs, temperature changes will cause the springs to bend without unduly stressing the mirror. In this case, rotational symmetry tends to keep the center of the mirror fixed in regard to the related optical system.[2,45]

Single-Point Diamond-Turned Mirrors And Mounts

Lathe or flycutting machines with carefully oriented single-crystal diamond-tipped tools are used to fabricate highly precise mounts for conventional (i.e., nonmetallic) mirrors or metallic mirrors with integral mounting provisions.[2,46-48] The process is commonly called single-point diamond turning (SPDT).

Figure 6.57 shows an example of a stainless steel mirror mount with precisely oriented internal pads to mechanically interface with a mirror made of low expansion material such as Zerodur® as well as equally precisely oriented external pads to interface with external structure. The mirror pads are integral with flexures formed in the mount itself by electrical discharge machining techniques. These flexures compensate for thermal expansion mismatch. The critical surfaces (pads) on the mount are all machined by SPDT techniques.

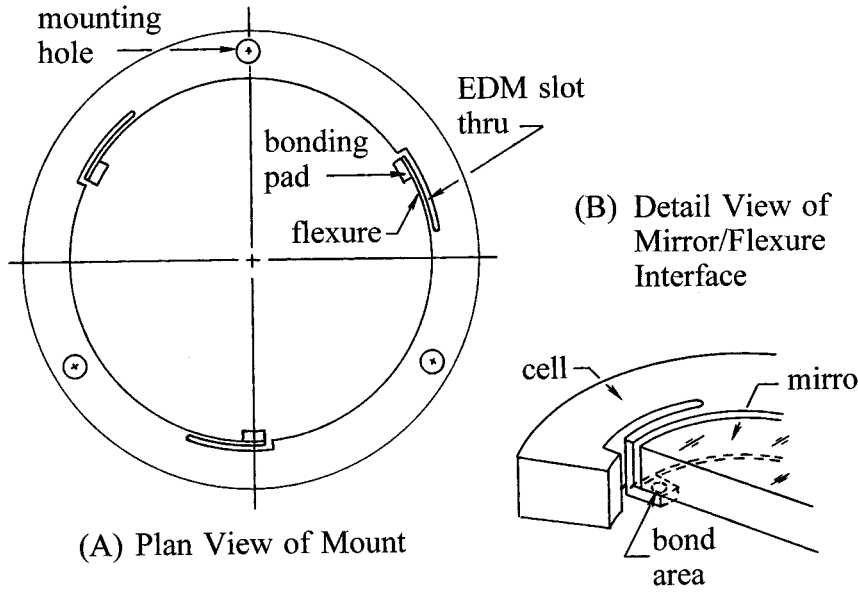

FIGURE 6.57 Concept for a rim-mounted mirror subassembly featuring integral flexure suspension means.

Figure 6.58 shows a metal mirror with integral shaft manufactured to close tolerances by SPDT techniques,[49] while Figure 6.59 shows a metal mirror with integral mount also fabricated by SPDT techniques to form an interchangeable module for a space-borne optical instrument.[50]

6.6 Mounts for Prisms

Clamped Mounts

Kinematic and Semikinematic Techniques

The position (translations) and orientation (tilts) of a prism generally must be controlled to tolerances dependent upon its location and function in the optical system. Control is accomplished through the prism's interfaces with its mechanical surround. The optical material should be placed in compression. Kinematic mounting avoids overconstraints that might distort the optical sur-

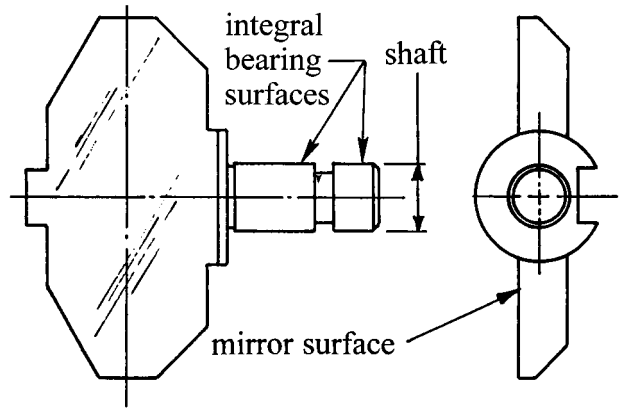

FIGURE 6.58 Metal mirror subassembly with integral gimbal axis fabricated by SPDT techniques. (Adapted from Addis, E.C. 1983. *Geometrical Optics, SPIE Proc. Vol. 389*, Taylor, W.H., ed., p. 36.)

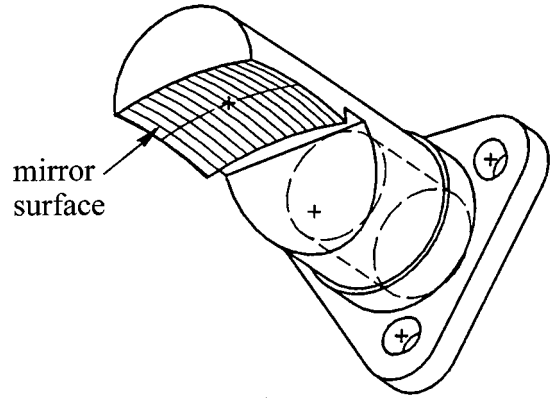

FIGURE 6.59 Diagram of a metal toroidal mirror subassembly with integral mount fabricated by SPDT technique. (Adapted from Visser, H. and Smorenborg, C. 1989. *Reflective Optics, SPIE Proc. Vol. 1113*, Korsch, D.G., ed., p. 65.)

faces.[2,10,51] Point contacts with high stresses inherent in true kinematic mounts are avoided by providing small area contacts at the interfaces.[2] Properly designed spring forces applied over these areas allow expansion and contraction with temperature changes while adequately constraining the prism against acceleration forces.[52] If contact is made on optically active surfaces, the contacting areas should be sufficiently flat and coplanar that surface deformations do not exceed the elastic deformations nominally caused by the clamping constraints.[10]

Figure 6.60 illustrates a semikinematic mounting for a cube-shaped beamsplitter prism. Here, five springs hold the prism against directly opposite pads. Although the contacts occur on refracting surfaces, they are located outside the used aperture, thereby minimizing the effects of surface distortions. This beamsplitter is used to divide a beam converging toward an image plane, each beam then forming an image on a separate detector. In order for these images to maintain their proper alignment relative to each other and to the structure of the optical instrument with temperature changes, the prism must not translate in the XY plane of the figure nor rotate about any of the three orthogonal axes. Translation in the Z direction has no effect. Once aligned, the prism must always press against the five areas indicated by the K_∞ symbols. Constraints are provided at the points labled K_i. The dashed outlines indicate how the prism will expand if the temperature increases. Registration of the prism surfaces against the locating/aligning pads does not change and the light paths to the detectors do not deviate.[52]

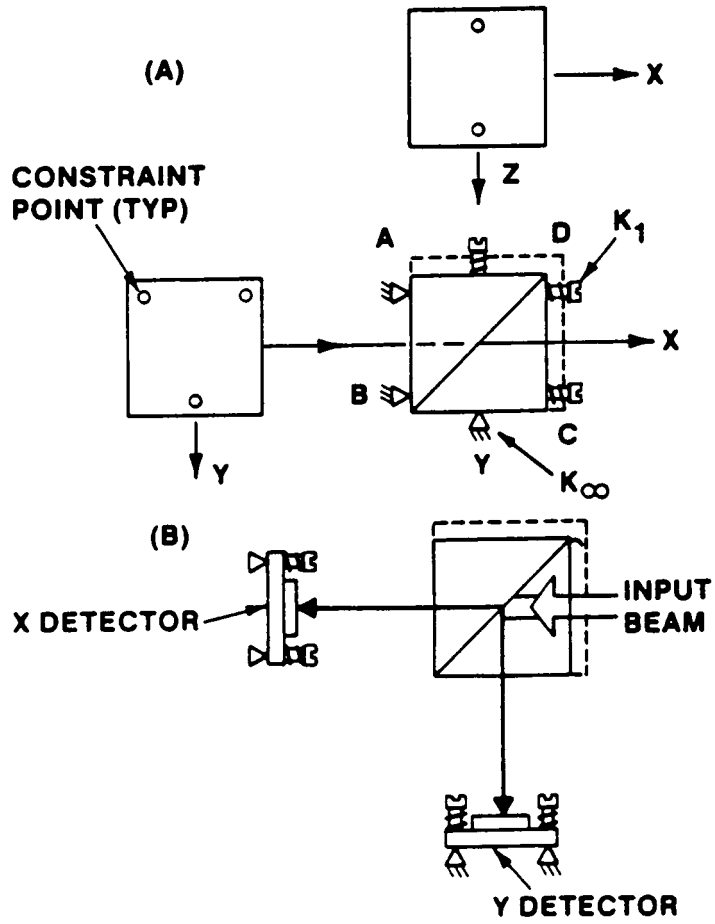

FIGURE 6.60 Schematic of a kinematic mounting for a cube-shaped, beamsplitter prism. (From Lipshutz, M.L. 1968. *Appl. Opt.*, 7, 2326.)

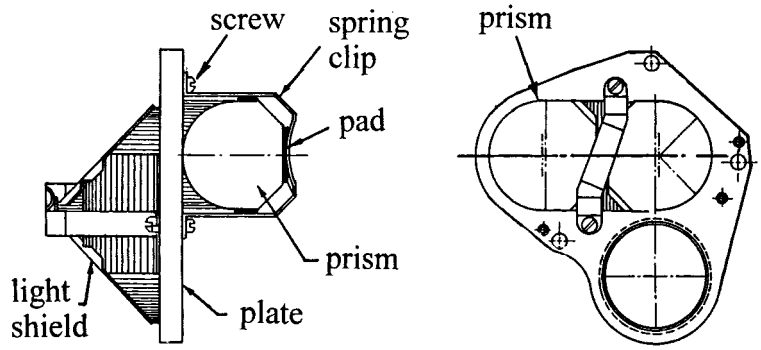

FIGURE 6.61 Schematic of a nonkinematic mounting for a Porro prism erecting subassembly. (Adapted from Yoder, P.R., Jr. 1985. *Geometrical Optics, SPIE Proc. Vol. 531*, Fischer, R.E., Price, W., and Smith, W.J., eds., p. 206.)

Nonkinematic Techniques

Spring or strap means are frequently used to hold prisms in place against the mounting interfaces in optical instruments. An example is the Porro prism erecting prism assembly shown schematically in Figure 6.61.[36] This is typical of prism mountings in binoculars or telescopes. Spring clips hold

each prism against a perforated mounting shelf that is, in turn, fastened with screws and locating pins to the instrument housing. Area contact occurs over large areas on the hypotenuse faces of the prisms, while lateral constraints are provided by recessing those faces slightly into opposite sides of the shelf.

Another example of the many types of nonkinematic mounts for prisms is shown in Figure 6.62. Here, an Amici prism is held by a flat spring clip against nominally flat reference pads inside the triangular housing of a military elbow telescope. Constraint perpendicular to the plane of the figure is provided by resilient pads attached to the ground sides of the prism; these are compressed when thin plate covers are attached with screws onto both sides of the housing. Note that the spring contacts the prism on the ground bevels at the ends of the roof surfaces. The spring is loaded against the prism by a screw threaded through the housing wall. The covers and the loading screw are all sealed to protect the environment within the telescope.[2]

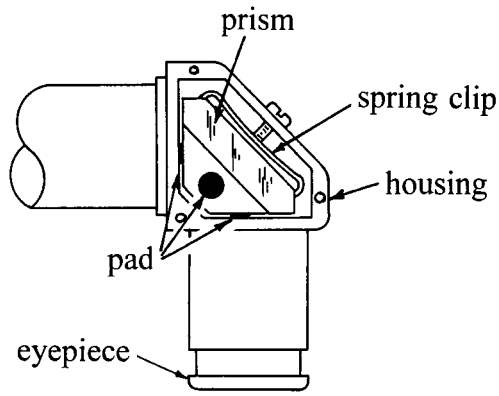

FIGURE 6.62 Schematic of a nonkinematic mounting for an Amici prism in a military elbow telescope.

Bonded Mounts

Many prisms are mounted by bonding their ground faces to mechanical pads using epoxy or similar adhesives. Contact areas large enough to render strong joints can usually be provided in designs with minimum complexity.

The critical aspects of the design are characteristics of the adhesive, thickness of the adhesive layer, cleanliness of the surfaces to be bonded, dissimilarity of coefficients of expansion of the materials, area of the bond, environmental conditions, and care with which the parts are assembled.[2] While the adhesive manufacturer's recommendations should be consulted, experimental verification of adequacy of the design, the materials to be used, the method of application, and cure conditions and duration are advisable in critical applications.

Guidelines for determining the appropriate bond area have appeared in the literature.[53] In general, the adhesive shear or tensile strength is ratioed to the product of prism weight and maximum expected acceleration divided by the bond area. If this ratio is greater than unity, some safety factor exists. This factor should be at least 2. Since adhesive layers normally shrink by a few percent of each dimension during curing, it is advisable to keep these dimensions as small as possible while providing adequate strength.

Examples of Cantilevered Techniques

Figure 6.63 illustrates a Porro prism bonded to a mechanical mounting surface in a cantilevered fashion. The prism is made of Schott SK16 glass, the mount is type 416 stainless steel, and the adhesive is 3M EC2216-B/A epoxy approximately 0.004 in. (0.1 mm) thick. The prism weight is 2.2 lb and the bond area (which covers the maximum area available on a ground face) is 5.6 in.^{2}. The intended military application expected the assembly to withstand 1500 G loading. Assuming

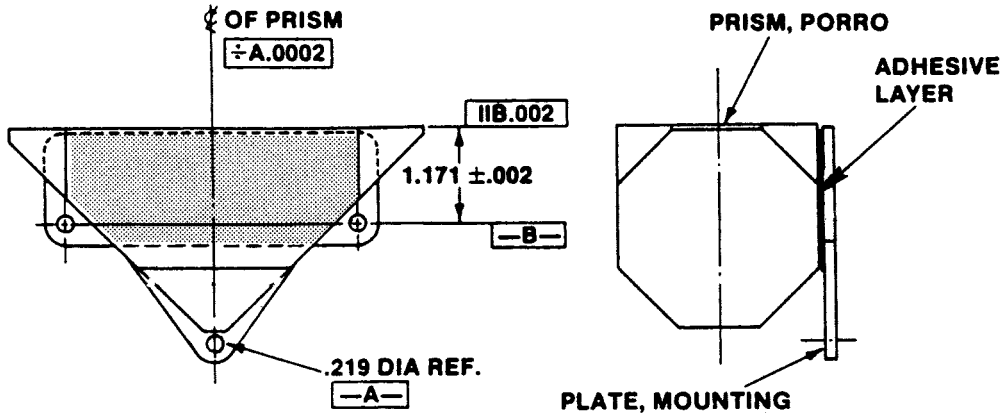

FIGURE 6.63 Schematic of a Porro prism bonded in cantilever fashion on full area (shaded) of one triangular ground face. Dimensions are inches. (Adapted from Yoder, P.R., Jr. 1985. *Geometrical Optics, SPIE Proc. Vol. 531*, Fischer, R.E., Price, W., and Smith, W.J., eds., p. 206.)

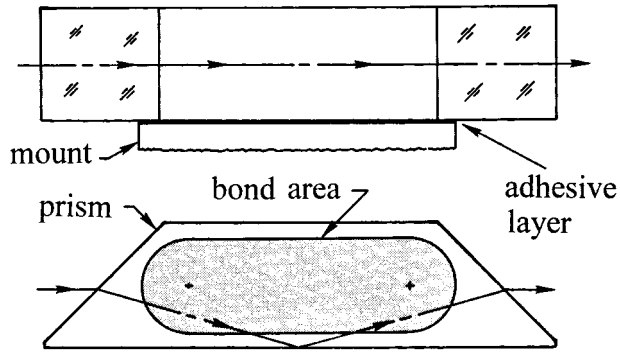

FIGURE 6.64 Schematic of a Dove derotation prism bonded in cantilever fashion on a racetrack-shaped area (shaded) of one ground face.

the adhesive strength to be 2500 lb/in.^{2}, the design safety factor would be 2500/[(2.2)(1500)/5.6] or 4.2. Tests of prototype hardware built to this design showed that it actually withstood 1200 G acceleration without failing. This at least partially confirmed the design.[36]

Figures 6.64 and 6.65 show two other designs for bonded assemblies with the prisms cantilevered from one surface. The former is a Dove prism in which the appropriate bond area has an elongated circle or "racetrack" shape. The latter is a Pechan prism comprised of two air-spaced elements with only one element bonded to the mount. It is best for an adhesive bond not to bridge over a discontinuity such as a cemented joint unless the elements are cemented together and the surfaces to be bonded were ground flat and coplanar after cementing. The latter example also illustrates division of a bond area into three subareas on the prism surface so as to reduce the lateral dimensions of the bond and thus to minimize the shrinkage effects. The three subareas are spaced as far apart as practical in order to stabilize the joint.

Examples of Multiple Support Techniques

Some designs for bonding prisms utilize multiple adhesive joints between the prism and structure as depicted in Figure 6.66. Here, an increased bond area and support from both sides are provided. It is necessary in such designs that the glass and metal surfaces at each interface be nearly parallel

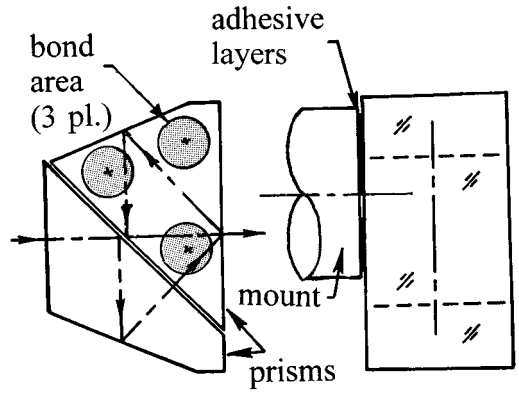

FIGURE 6.65 Schematic of a Pechan derotation prism subassembly bonded in cantilever fashion on multiple circular areas (shaded) of one ground face.

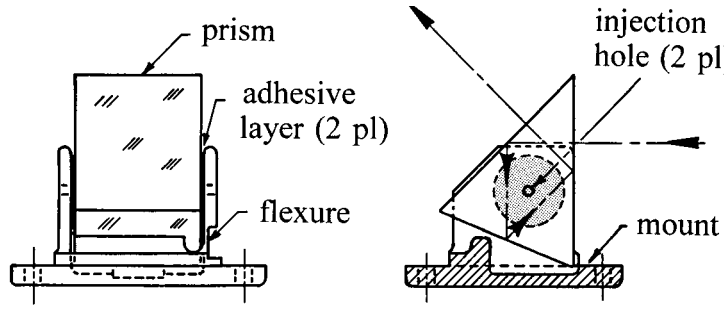

FIGURE 6.66 Schematic of Schmidt prism supported from both sides by bonded areas. (From Willey, R., private communication.)

and that the proper clearances be provided for insertion of the adhesive layers. Tolerances must be held closely enough to ensure these relationships.

Problems with differential expansion of metal and glass at extreme temperatures were avoided in this design by building a flexure into one support arm. Early models without this flexure were damaged at low temperature when the mount contracted more than the prism, causing the arms to pivot about the bottom edge of the prism, and pull away from the prism at the top of the bonds. Allowing the arm to bend slightly prevented such damage.[54]

Another design with support rendered from two sides is shown in Figure 6.67. In this case, the prism is bonded to a pad on one support arm (at left) and to the metal plug shown protruding through, but not attached to the right arm. Alignment of the prism is accomplished using mechanical references or optical fixturing during this first bonding step. After these first bonds have cured, the plug is epoxied to the right arm. With this approach, tolerances on location and tilt of the surfaces to be bonded can be relaxed, since the plug aligns itself to the prism before it is bonded to the arm.

Flexure Mounts

Some prisms (particularly large ones or ones with critical positioning requirements) are conveniently mounted by way of flexures. An example is shown in Figure 6.68.[2] Here, a large prism of unspecified shape is bonded to two cylindrical posts with multiple "necked-down" regions forming "universal joints" to compensate for nonparallelism between the surfaces to be bonded. Cruciform-shaped torsion flexures allow relative rotational motions. Temperature changes will not distort the

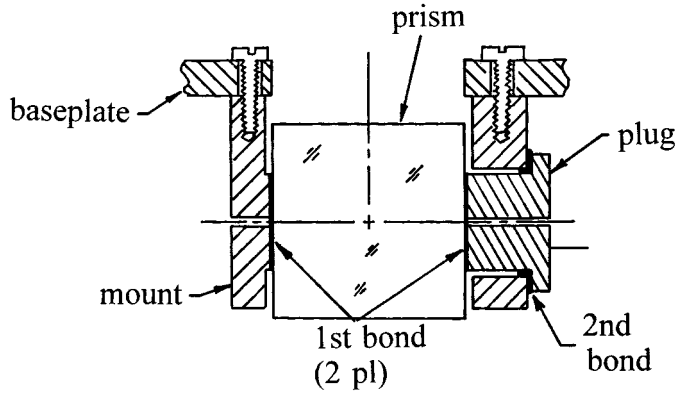

FIGURE 6.67 Schematic of another two-sided prism mount featuring two-step bonding to facilitate alignment without imposing tight tolerances.

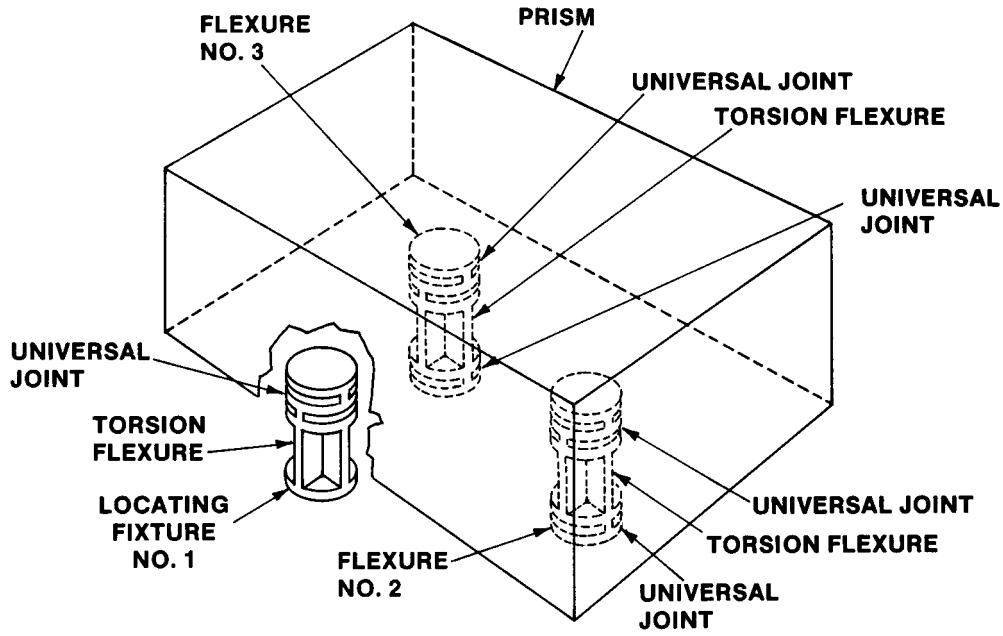

FIGURE 6.68 Schematic representation of a multiflexure mount for a large prism. (From Yoder, P.R., Jr. 1993. *Opto-Mechanical Systems Design*, 2nd ed. Marcel Dekker, New York.)

prism even if the thermal expansion coefficients of the prism, its mount, and the supporting structure are significantly different.

References

1. Smith, W. J. 1990. *Modern Optical Engineering*, 2nd ed., chap. 14. McGraw-Hill, New York.
2. Yoder, P. R., Jr. 1993. *Opto-Mechanical Systems Design*, 2nd ed., Marcel Dekker, New York.
3. Yoder, P. R., Jr. 1993. Lens mounting techniques. In *Optical Systems Engineering III, SPIE Proc. Vol. 389*, Taylor, W. H., ed., p. 2.
4. Horne, D. F. 1972. *Optical Production Technology.* Adam Hilger, Bristol, England.
5. Jacobs, D. H. 1943. *Fundamentals of Optical Engineering.* McGraw-Hill, New York.
6. Bayar, M. 1981. Lens barrel optomechanical design principles, *Opt. Eng.*, 20, 181.

7. Hopkins, R. E. 1980. Lens mounting and centering, chap. 2. In *Applied Optics and Optical Engineering, Vol VIII*. Academic Press, New York.
8. Kowalskie, B. J. 1980. A user's guide to designing and mounting lenses and mirrors, p. 98. In *Digest of Papers, OSA Workshop on Optical Fabrication and Testing*. North Falmouth.
9. Roark, R. J. 1954. *Formulas for Stress and Strain*, 3rd ed., McGraw-Hill, New York,
10. Ritchey, C. A. 1974. Aerospace mounts for down-to-earth optics, *Machine Design*, 46, 121.
11. Vukobratovich, D. 1993. Optomechanical systems design, chap. 3. In *The Infrared & Electro-Optical Systems Handbook, Vol. 4*, Dudzik, M. C., ed. ERIM, Ann Arbor and SPIE, Bellingham.
12. Delgado, R. F. and Hallinan, M. 1975. Mounting of optical elements, *Opt. Eng.*, 14, S-11.
13. Yoder, P. R., Jr. 1991. Axial stresses with toroidal lens-to-mount interfaces. In *Optomechanics and Dimensional Stability, SPIE Proc. Vol. 1533*, Paquin, R. A. and Vukobratovich, D., eds., p. 2.
14. Yoder, P. R., Jr. 1993. Parametric investigations of mounting-induced axial contact stresses in individual lens elements. In *Optomechanical Design, SPIE Proc. Vol. 1998*, Vukobratovich, D., Yoder, P. R., Jr., and Genberg, V., eds., p. 8.
15. Walker, B. H. 1993. 'Select' optical glasses, p. H-356. In *The Photonics Design and Applications Handbook*. Laurin Publishing, Pittsfield, MA.
16. *Optical Glass Catalog 3111e*, Schott Glass Technologies, Inc., Duryea, PA.
17. Yoder, P. R., Jr. 1994. Estimation of mounting-induced axial contact stresses in multi-element lens assemblies. In *Current Developments in Optical Design and Engineering, SPIE Proc. Vol. 2263*, Fischer, R. E. and Smith, W. J., eds, p. 386.
18. Hatheway, A. E. 1993. Analysis of adhesive bonds in optics. In *Optomechanical Design, SPIE Proc. Vol. 1998*, Vukobratovich, D., Yoder, P. R., Jr., and Genberg, V. L., eds., p. 2.
19. Valente, T.M. and Richard, R.M. 1991. Analysis of elastomer lens mountings. In *Optomechanics and Dimensional Stability, SPIE Proc. Vol. 1533*, Paquin, R. A. and Vukobratovich, D., eds., p. 21.
20. Yoder, P. R., Jr. 1992. Advanced considerations of the lens-to-mount interface. In *Optomechanical Design, SPIE Proc. CR43*, Yoder, P. R., Jr., ed., p. 305.
21. Betinsky and Welham. 1979. Optical design and evaluation of large aspherical-surface plastic lenses. In *Optical Systems Engineering, SPIE Proc. Vol. 193*, Yoder, P. R., Jr., ed., p. 78.
22. Yoder, P. R., Jr. 1986. Optomechanical designs of two special purpose objective lens assemblies. In *Contemporary Optical Instrument Design, Fabrication, Assembly and Testing, SPIE Proc. Vol. 656*, Beckmann, L. H. J. F., Briers, J. D., and Yoder, P. R., Jr., eds., p. 225.
23. Scott, R. M., Optical engineering, *Appl. Opt.*, 1, 387.
24. Yoder, P. R., Jr. 1972. A low-light level objective lens with integral laser channel, *Opt. Eng.*, 11, 127.
25. Hopkins, R. E., 1976. Some thoughts on lens mounting, *Opt. Eng.*, 15, 428.
26. Carnell, K. H., Kidger, M. J., Overill, M. J., Reader, A. J., Reavell, F. C., Welford, W. T., and Wynne, C. G. 1974. Some experiments on precision lens centering and mounting, *Opt. Acta*, 21, 615.
27. Fischer, R. E. 1991. Case study of elastomeric lens mounts. In *Optomechanics and Dimensional Stability, SPIE Proc. Vol. 1533*, Paquin, R. A. and Vukobratovich, D., eds., p. 27.
28. Valente T. M. and Richard, R. M. 1994. Interference fit equations for lens cell design using elastomeric lens mountings, *Opt. Eng.*, 33, 1223.
29. Yoder, P. R., Jr. 1960. Two new lightweight military binoculars, *J. Opt. Soc. Am.*, 50, 491.
30. Trsar, W. J., Benjamin, R. J., and Casper, J. F. 1981. Production engineering and implementation of a modular military binocular, *Opt. Eng.*, 20, 201.
31. 1983. *The Handbook of Plastic Optics*, 2nd ed., U.S. Precision Lens, Inc., Cincinnati, OH.
32. Ashton, A. 1979. Zoom lens systems, *Int. Semin. Adv. Opt. Prod. Technol. SPIE Proc. Vol. 163*, p. 92.

33. Parr-Burman, P. and Gardam, A. 1985. The development of a compact IR zoom telescope. In *Infrared Technology and Applications, SPIE Proc. Vol. 590*, Baker, L. R. and Masson, A., eds., p. 11.
34. Kampe, T. U. and Johnson, C. W. 1989. Optomechanical design considerations in the development of the DDLT laser diode collimator. In *Optomechanical Design of Laser Transmitters and Receivers, SPIE Proc. Vol. 1044*, Seery, B. D., ed., p. 46.
35. Quammen, M. L., Cassidy, P. J., Jordan, F. J., and Yoder, P. R., Jr. 1966. Telescope Eyepiece Assembly with Static and Dynamic Bellows-Type Seal, U.S. Patent No. 3,246,563.
36. Yoder, P. R., Jr. 1985. Non-image-forming optical components. In *Geometrical Optics, SPIE Proc. Vol. 531*, Fischer, R. E., Price, W., and Smith, W. J., eds., p. 206.
37. Manuccia, T. J., Peele, J. R., and Geosling, C. E. 1981. High temperature ultrahigh vacuum infrared window seal, *Rev. Sci. Instrum.*, 52, 1857.
38. Stoll, R., Forman, P. F., and Edleman, J. 1961. The effect of different grinding procedures on the strength of scratched and unscratched fused silica, p. 1. In *Proc. Symp. Strength of Glass and Ways to Improve It.* Union Scientifique Continentale du Verre, Charleroi, Belgium.
39. Robinson, B., Eastman, D. R., Bacevic, J., and O'Neill, B. J. 1983. Infrared window manufacturing technology. In *Infrared Technology IX, SPIE Proc. Vol. 430*, Spiro, I. J., ed., p. 302.
40. Klein, C. A., diBenedetto, B., and Pappis, J. 1986. ZnS, ZnSe and ZnS/ZnSe windows: their impact on FLIR system performance, *Opt. Eng.*, 25, 519.
41. Speare, J. and Belloli, A. 1983. Structural mechanics of a mortar launched IR dome. In *Structural Mechanics of Optical Systems, SPIE Proc. Vol. 450*, Cohen, L. M., ed., p. 182.
42. Vukobratovich, D. 1986. *Introduction to Optomechanical Design, SPIE Short Course Notes.*
43. Dunn, G. and Stachiw, J. 1966. Acrylic windows for underwater structures. In *Underwater Photo-Optics, SPIE Proc. Vol. 7*, p. D-XX-1.
44. Barnes, W. P., Jr. 1966. Some effects of aerospace thermal environments on high-acuity optical systems, *Appl. Opt.*, 5, 701.
45. Hookman, R. 1989. Design of the GOES telescope secondary mirror mounting. In *Precision Engineering and Optomechanics, SPIE Proc. Vol. 1167*, Vukobratovich, D., ed., p. 368.
46. Saito, T. T. 1978. Diamond turning of optics: the past, the present and the exciting future, *Opt. Eng.*, 17, 570.
47. Gerchman, M. 1986. Specifications and manufacturing considerations of diamond-machined optical components. In *Optical Component Specifications for Laser-Based Systems and Other Modern Optical Systems, SPIE Proc. Vol. 607*, Fischer, R. E. and Smith, W. J., eds., p. 36.
48. Sanger, G. M. 1987. The precision machining of optics. In *Applied Optics and Optical Engineering, Vol. 10*, Shannon, R. R. and Wyant, J. C., eds., chap. 6, Academic Press, New York.
49. Addis, E. C. 1983. Value engineering additives in optical sighting devices. In *Geometrical Optics, SPIE Proc. Vol. 389*, Taylor, W. H., ed., p. 36.
50. Visser, H. and Smorenborg, C. 1989. All reflective spectrometer design for Infrared Space Observatory. In *Reflective Optics, SPIE Proc. Vol. 1113*, Korsch, D. G., ed., p. 65.
51. Durie, D. S. L. 1968. Stability of optical mounts. In *Machine Des.,* 40, 184.
52. Lipshutz, M. L. 1968. Optomechanical considerations for optical beamsplitters, *Appl. Opt.*, 7, 2326.
53. Yoder, P. R., Jr. 1988. Design guidelines for bonding prisms to mounts. In *Optical Design Methods, Applications, and Large Optics, SPIE Proc. Vol. 1013*, Masson, A., Schulte in den Bäumen, J., and Zügge, H., eds., p. 112.
54. Willey, R., private communication.